Author Manuscript

Locally Derived, Meteoric Fluid Infiltration was Responsible for Widespread Late Paleozoic Illite Authigenesis in the Appalachian Basin

A. Boles (ORCID: 0000-0003-3072-3309)[1] and B. van der Pluijm (ORCID: 0000-0001-7737-2791)[1]

[1] Department of Earth and Environmental Sciences, University of Michigan, Ann Arbor, MI, USA

Corresponding author: Austin Boles (aboles@umich.edu)

Key Points:

- Far-field stress due to Alleghanian orogenesis facilitates reorganization of architecture and fluid pathways of the brittle crust and drives regional diagenesis.
- Evidence for locally sourced, surface-derived fluid challenges popular hypothesis of orogenic fluid expulsion.
- Pairing of stable and radiogenic isotope analysis of authigenic illite constrains the relationship between regional diagenesis and tectonism.

This is the author manuscript accepted for publication and has undergone full peer review but has not been through the copyediting, typesetting, pagination and proofreading process, which may lead to differences between this version and the Version of Record. Please cite this article as doi: 10.1029/2020TC006137

This article is protected by copyright. All rights reserved.

Author Manuscript

Abstract

Isotopic and geochronologic investigation of authigenic, K-bearing clays in the Appalachian Plateau of the northeastern US Midcontinent yields new insights about the tectonic and diagenetic history of the North American sedimentary cover sequence. In-situ texture analysis by High Resolution X-ray Texture Goniometry indicates preservation of bedding-parallel diagenetic fabrics with burial depths of 2-5 km, and illite mineralization temperatures are spatially variable, ranging from 80-190ºC, correlating to similar depths of 3-6 km. The mineralizing geofluid is surface-derived, with δD values ranging from -48 to -72‰ (in the range of predicted Pangea meteoric fluid). In addition, we find that mineralizing fluid δD values increase away from the orogenic front, consistent with a rain shadow effect from the high elevation Appalachian orogen. The age of authigenic illite is constrained by $^{40}Ar/^{39}Ar$ geochronology to 308-318 Ma, reflecting Upper Carboniferous diagenesis. We postulate that far-field stress transmission from continent-continent collision created regional permeability pathways for surface fluids, altering the hydrologic architecture of the brittle crust and allowing meteoric fluid infiltration into upper crustal rocks. This interpretation challenges the popular view of tectonically forced, lateral fluid flow from the Appalachian orogen ("squeegee hypothesis").

1 Introduction

The theory of plate tectonics divides the lithosphere (the crust and upper mantle) into thin, rigid blocks that interact with one another at their boundaries (Morgan, 1968). Within this powerful framework, however, intraplate deformation can also occur in continental and oceanic settings (Molnar, 1988). Examples include the Central Indian basin, a 3,000 km wide deformation zone in the Indian Ocean (Neprochnov et al., 1988; Bull, 1990; Singh et al., 2017), and the Ancestral Rockies, Laramide, orogeny, and intracratonic basins of the North American craton (e.g. van der Pluijm et al., 1997; Marshak et al., 2000). The existence of intraplate deformation, and the memory of the stress field retained by the rocks (e.g. van der Pluijm et al., 1997), indicate that far-field stresses from boundary-zone deformation belts are transferred deep into cratonic interiors. The orientation, style, and magnitude of the diffuse strain experienced by the plate is often determined, or filtered, by preexisting structures in basement rock (Craddock et al., 1993; Marshak et al., 2000). The intraplate, brittle crust remains strong through a process of

This article is protected by copyright. All rights reserved.

faulting and fluid movement by maintaining a state of critical stress, near-hydrostatic pore pressures, and high permeability (Townend and Zoback, 2000; Zoback and Townend, 2001).

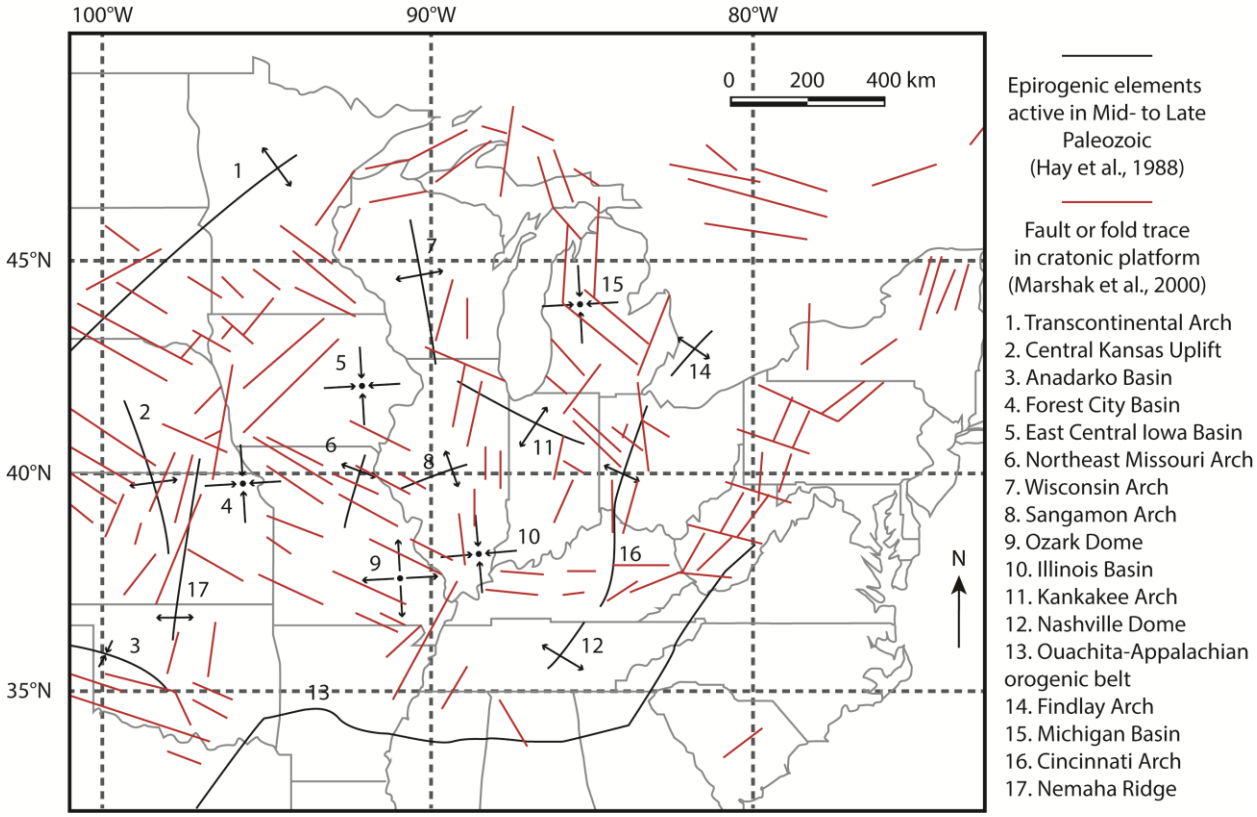

Figure 1 Structural features of the North American midcontinent that include both epeirogenic elements and basement faults and folds. Modified after Hay et al. (1988) and Marshak et al. (2000).

One manifestation of intraplate deformation, epeirogeny—long-wavelength, vertical movements in cratonic settings - is particularly widespread in the North American midcontinent (figure 1). In addition to domes, arches, and basins, many through-going discontinuities have been identified in the basement rocks of the eastern United States (Hay et al., 1988; Marshak et al., 2000). Although the kinematics of such structural features remain a topic of debate, their existence and ubiquity are striking. Many have been temporally linked to plate boundary deformation, diagenesis, and fluid flow (e.g. Bethke, 1986; Grathoff et al., 2001; Carlson, 1994).

The long-range mobilization of fluids in foreland basin sedimentary cover due to tectonic activity was first postulated by Oliver (1986). In this conceptual model, orogenesis promotes sediment compaction deep within the foreland basin wedge, while inducing laterally migrating, high-temperature, and solute-rich basinal brine migration away from the orogen. It has provided a simple and compelling explanation for several geologic phenomena in the North American

This article is protected by copyright. All rights reserved.

Author Manuscript

Author Manuscript

midcontinent, including brine-derived Mississippi Valley-type (MVT) ore deposits (Hearn et al., 1987), regional potassium metasomatism (Buyce and Friedman, 1975; Elliott and Aronson, 1987; Lu et al., 1991; Schedl et al., 1993), anomalously high thermal histories of shallowly buried sediments (Cathles and Smith, 1983; Sverjensky, 1986), correlation of hydrocarbon accumulations to distant source rocks (Momper, 1978; Clayton and Swetland, 1980), and widespread paleomagnetic remagnetization (Miller and Kent, 1988; McCabe et al., 1989; Manning and Elmore, 2012; Vander Voo and Torsvik, 2012). However, direct testing of this powerful fluid migration hypothesis has been challenging.

Bethke and Marshak (1990) examined the lines of evidence in detail and concluded that brine migrations can achieve the length scale of an orogenic belt and transfer geofluid many hundreds of kilometers into plate interiors (see also Garven, 1995; Person and Baumgartner, 1995 for reviews). Several other observations, however, challenge the claim that warm geofluid can flow laterally within a sedimentary package across such distances:

(1) The structurally induced permeability anisotropy of the deformed rock that is expected for a compressional system is predicted to preferentially direct a significant proportion of fluid flow along strike; i.e., parallel—not perpendicular—to the orogen (Sibson, 2005).

(2) Fluid flow, regardless of the forcing mechanism, will always be down hydraulic gradients, but competition between deformation processes which maintain connectivity and those which close pathways will determine permissible fluid volumes and flow rates (Knipe and McCaig, 1994). In compressional sedimentary systems at low temperatures, permeability restriction by pressure solution, compaction, and cementation is likely to be greater than permeability enhancement by the opening of fractures and grain-boundary voids or chemical dissolution.

(3) Primary permeability distribution is anisotropic, and highly dependent on sedimentary facies (Bjorlykke, 1993). Adherence to Walther's Law ("…only those facies and facies-areas can be superimposed primarily which can be observed beside each other at the present time"; Middleton, 1973) suggests lateral primary permeability variations that would significantly affect horizontal flow. Moreover, these variations and the observed mineral reactions would require flow rates and durations of flow that are not attainable by

This article is protected by copyright. All rights reserved.

compaction-driven flow without extreme focusing of that flow, which precludes regional alteration events (Schedl, 1992; Bjorlykke, 1994).

(4) Time-dependent numerical models of fluid, heat- and solute transport indicate that the high fluid velocities required to carry heat to basin margins rapidly exhausts solute supply provided by compaction-driven flow (Deming et al., 1990; Deming and Nunn, 1991). This mechanism can, therefore, only explain regional brine migration if flow is focused into spatially restricted discharge zones and sets fundamental limitations on the ability of either compaction-driven or topographically driven flow to continuously transport significant heat across a basin for an extended period of time (Nunn and Deming, 1991).

(5) A model assuming a single hydrostratigraphic system that dominates the whole of the Appalachian basin is simplistic, and the reality is likely an interplay between several flow systems, each competing, mixing, and interfering with the others (Bachu, 1995).

Presenting new data on the ancient fluid source for regional illitization, the current study challenges the "orogenic squeegee" concept by examining potassium metasomatism that is widespread in the North American midcontinent. We utilize recent advances in the illite polytype analysis method to delimit the diagenetic age of illite and its geofluid source from hydrogen isotopic composition in mudstone across the northern Appalachian basin. We conclude—based on the results of age analysis and fluid composition—that pre-existing structural features and intracratonic stress mobilized locally sourced, surface-derived fluid and lead to widespread and protracted diagenesis within the continental sedimentary cover of the Appalachian Plateau. The introduction of a locally sourced surface fluid resolves problems related to long-range fluid mobilization (fluid volume and temperature), while the timing of illitization maintains the connection between foreland and orogenic deformation.

2 Geologic Background

The Appalachian Plateau is a tectonic province of the central Appalachian orogenic belt that is characterized by flat-lying to gently folded Paleozoic strata that were deposited in a foreland basin (Quinlan and Beaumont, 1984; Mitra, 1987; Hatcher, 2010). 44 mudstone samples were collected in this region (Figure 2). Sample location GPS coordinates are included in the System for Earth Sample Registration (SESAR) repository (see Figure 2 for International Geo Sample

This article is protected by copyright. All rights reserved.

Author Manuscript

Numbers, IGSN's). Fine-grained lithologies were targeted to maximize the clay content for illite polytype analysis. About 2 kg of sample was collected at each location, from beneath any modern soil to avoid recent contamination. Two transects of the Appalachian Plateau, oriented orthogonally to the Appalachian Mountains in New York and Ohio, West Virginia, and Pennsylvania were targeted. Additional sampling in the Valley and Ridge Province in central Pennsylvania was conducted to gain lateral continuity of samples representing undeformed to highly strained material. Thus, the sample suite represents a variety of rock types (shale, siltstone, argillaceous limestone) that range from Early to late Paleozoic age.

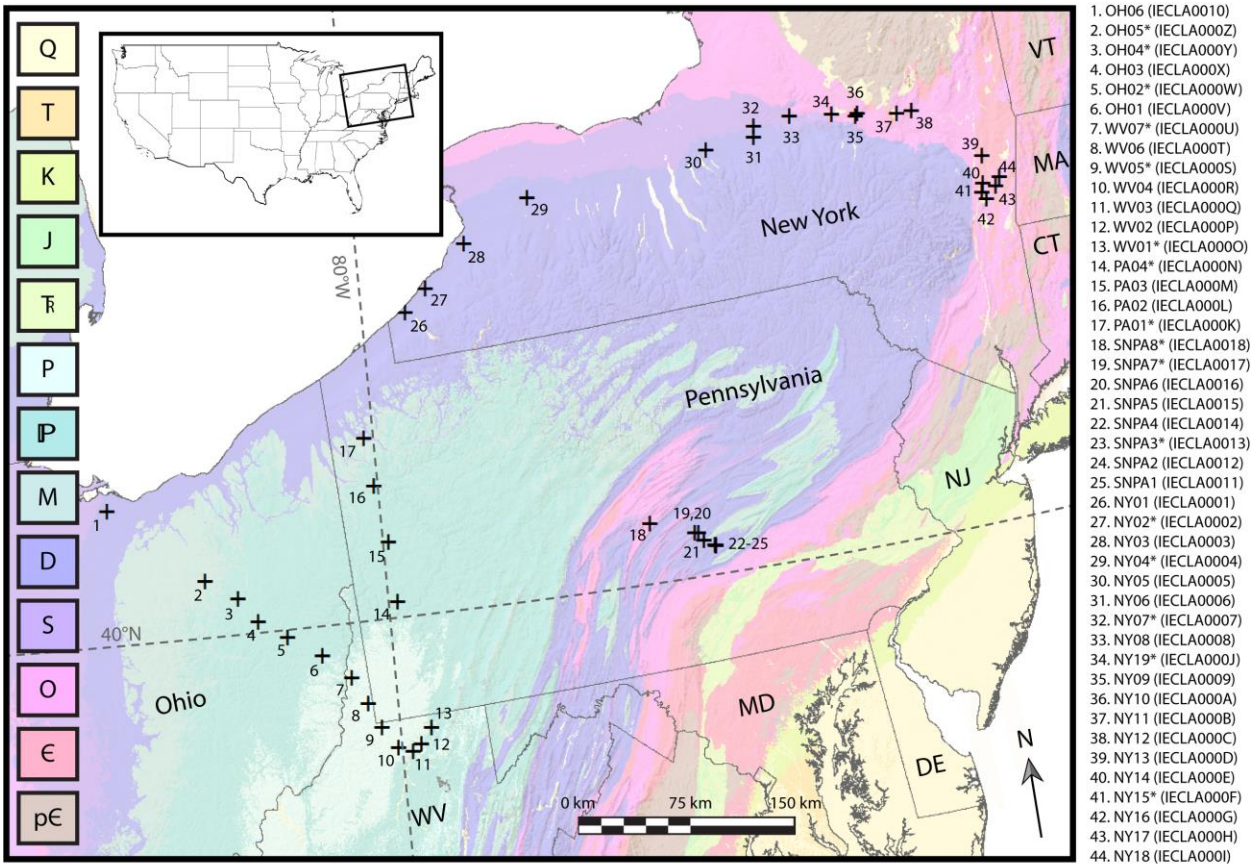

Figure 2 Generalized geologic map of the Northern Appalachian basin. Mudstone surface sample locations used in this study are denoted with cross symbols. IGSN's are listed with sample names.

3 Materials and Methods

High resolution X-ray texture goniometry is utilized in this study to determine the presence of a diagenetic rock fabric. Illite polytype analysis for both H isotopic composition and Ar radiometric ages are utilized to determine the timing of diagenesis and the nature of the mineralizing fluids in the diagenetic environment at the time of illite authigenesis. H isotopic

This article is protected by copyright. All rights reserved.

Author Manuscript

Author Manuscript

analysis was selected over O isotopic analysis, because fluid tends to equilibrate with the abundantly O-rich constituents of host rock during passage (Fitz-Diaz et al., 2011).

3.1 X-ray Texture Goniometry

X-ray texture goniometry (XTG) was conducted on an ENRAF-Nonius CAD4 automated single-crystal diffractometer using a Mo source, operated at 23 mA and 43 kV, and located in the University of Michigan's Electron Microbeam Analysis Laboratory (van der Pluijm et al., 1994). By using transmission mode, crystallographic preferred orientation is measured, and a pole figure generated for the 1 nm 001 d-spacing of the clay mineral illite. A multiple of random distribution (MRD) value is also calculated that quantifies crystallite misorientation. The resultant magnitude of such a misorientation distribution MRD value describes the calculated probability of illite misorientation with respect to a material with uniformly distributed misorientations (an MRD value equal to 1 is a perfectly random distribution; higher MRD values indicate greater levels of anisotropy or crystallographic preferred orientation).

The samples were first investigated over a 2θ range of 0.5-6.0º (corresponding to 1-13º2θ Cu) to determine the exact diffraction angle at which textural data should be collected. Next, a "pole-figure scan" (Ho et al., 1995) was completed wherein diffracted X-ray intensity data are collected every 2.5º from 0-360º along an axis parallel to a line between the goniometer and the detector, and in 9 steps between 0-40º around a second axis oriented normal to the first. A total of 1296 intensity measurements are made, corrections are made for sample absorption, grain density, and specimen thickness, and intensity data are smoothed, rotated, and displayed on pole figure diagrams (van der Pluijm et al., 1994). Eight samples were selected for XTG analysis representing two transects west of the Appalachian orogen in New York and West Virginia. A 0.2-0.5 mm thick section of each sample was prepared so that X-rays are transmitted through the sample in an orientation parallel to bedding.

3.2 Hydrogen Isotopes

δD values were measured at the Joint Goethe University – BiK-F Stable Isotope Facility Frankfurt using a ThermoFinnigan MAT 253 mass spectrometer in continuous flow mode coupled to a high temperature conversion elemental analyser (TC-EA). A sample weight of 1 mg was wrapped into Ag foil and dried overnight at 150°C in a stainless-steel tray. Samples were

This article is protected by copyright. All rights reserved.

rapidly transferred to a zero-blank autosampler that was immediately purged with helium gas to avoid re-hydration with ambient air moisture. Standards were run in-line with unknowns and reproduced with an error below ±2 ‰. All δD values are reported relative to standard mean ocean water (VSMOW). The fractionation equation of Capuano (1992) was utilized for 1Md illite, and the chlorite fractionation equation of Graham et al. (1987) was used with an anchizone-greenschist facies temperature of 300°C to obtain the mineralizing fluid compositions of the equilibrium solids.

3.3 $^{40}Ar/^{39}Ar$ Geochronology

Ar isotope analysis was conducted at the University of Michigan's Noble Gas Laboratory. Vacuum encapsulated samples were irradiated for 90 MWh at location 8C of the McMaster Nuclear reactor at McMaster University in Hamilton, Ontario, in irradiation package mc53. Each capsule had a packet of standard mineral MMhb-1 placed above and below the capsule. Measurement procedures for encapsulated clay samples follow the procedures outlined in Hall (2013). Vacuum capsules were made from 2 mm outer-diameter, 1 mm inner-diameter fused silica (i.e. quartz) tubing. Sections of tubing were cut into 10 cm-long segments and each segment was heated in the middle with a methane-O_2 torch while pulling apart each half, thereby collapsing the center into two 5 cm long pieces with break-seal tips.

Clay samples were first suspended in 1 mL of deionized water and centrifuged in a 1.5 mL tube. The water was then decanted and the remaining clay pellet was allowed to dry in a laminar flow hood. Small (~0.5 mg) pieces of the clay pellets were cut from the dried pellet and loaded into the quartz break-seal tubes and then attached to a vacuum manifold. Procedures for evacuating the break-seal tubes and analyzing the encapsulated samples are outlined in detail in Hall (2013). Encapsulated samples were not baked prior to analysis in order to reduce the possibility of outgassing the sample, thereby complicating the measurement of Ar release due to recoil effects. Encapsulated samples were laser step-heated in situ until complete fusion was achieved using a defocused beam from a 5 W Coherent Innova continuous Ar-ion laser operated in multi-line mode. For each degassing step, the system was programmed to heat each grain in turn for 60 seconds.

Ar isotopes were measured using a VG1200S mass spectrometer with a source operating at 150 μA total emission and equipped with a Daly detector operating in analog mode. Mass

This article is protected by copyright. All rights reserved.

Author Manuscript

discrimination was monitored daily using ~4x10^9 ccSTP of atmospheric Ar. Fusion system blanks were run every five fusion steps and blank levels from argon masses 36 through 40 (~2 x 10^{14}, ~3 x 10^{14}, ~1 x 10^{14}, ~3 x 10^{14}, and 2 x 10^{12} ccSTP respectively) were subtracted from sample gas fractions. Corrections were also made for the decay of ^{37}Ar and ^{39}Ar, as well as interfering nucleogenic reactions from K, Ca, and Cl as well as the production of ^{36}Ar from the decay of ^{36}Cl. Standard hornblende MMhb-1 was used as a neutron fluence monitor with an assumed age of 520.4 Ma (Samson and Alexander, 1987). The utilization of either total gas or retention age is determined by crystallite thickness; total gas ages are used in this study as is typical for fine-grained 1Md illite material (Hnat and van der Pluijm, 2014; Fitz-Díaz et al., 2016).

3.4 Illite Polytype Analysis

The illite polytype analysis method utilizes quantitative X-ray powder diffraction (Q-XRPD) techniques to appraise relative proportions of low- and high-temperature illite polytype end-members in a plurality of grain-sizes of a single sample for the purpose of unmixing the isotopic signals of coexisting illite populations in natural rocks (van der Pluijm et al., 2001; van der Pluijm and Hall, 2015). Quantitative examination of illite polytypes is possible by X-ray diffraction, as polytypism is expressed as differences in layer stacking patterns, leading to distinct hkl reflections for each polytype. The 2M1 polytype is a higher temperature, well-ordered phase that is typically detrital (metamorphic) in origin in low-grade sedimentary rocks. The 1Md polytype is a low-temperature, disordered phase that has a secondary (diagenetic) origin. A quantitative assessment of polytype proportions and an isotopic measurement are acquired for each grain-size aliquot of a sample. These are then correlated using York-type linear regression (Mahon, 1996) and the extrapolated end-member values represent the unmixed illite population isotopic compositions.

X-ray diffraction was conducted using a Rigaku Ultima IV diffractometer equipped with CuKα radiation, operated at 40 kV and 44 mA, and located in the Electron Microbeam Analysis Laboratory at the University of Michigan. Oriented slides were measured in both air-dried and ethylene glycolated conditions for qualitative assessment. The front-loading method for random preparations was used for quantitative characterization (Moore and Reynolds, 1997).

This article is protected by copyright. All rights reserved.

Author Manuscript

Author Manuscript

Rietveld whole-pattern matching software BGMN® was used for quantitative analysis (Bergmann et al., 1998). As shown recently (Boles et al., 2018), the Rietveld method for illite polytype quantification is superior to other quantification methods for mixed samples, as the proportions of additional populations of hydrous clay phases can be quantified. This approach also yields more robust error statistics (<±2%) and removes user dependency (Kleeberg, 2009).

The recent successes in utilizing the H isotopic composition of illite (Boles et al., 2015) and the implementation of Rietveld analysis for Q-XRPD (Boles et al., 2018) have broadened the scope and increased the accuracy and ease of illite polytype analysis.

To create H mixing plots, weight percent 1Md illite is normalized by the total weight percent of all hydrous minerals (γ) using equation 1:

$$\gamma = (\%1Md\ illite)/((\%\ 1Md\ illite + \%\ 2M1\ illite + \%\ chlorite + \%\ other\ hydrous\ minerals)) * 100 \quad (1)$$

The extrapolated endmembers are 1Md illite at one extremity, and a high-T aggregate signal of 2M1 illite, chlorite, and other hydrous phases at the other. Compellingly linear correlation indicates that the high-T clay phases all have the same isotopic composition; it is highly unlikely that varying proportions of each mineral constituent in each size fraction would produce bulk isotopic measurements that correlate linearly with grain-size. In the majority of samples, this signal is dominated by chlorite.

A total of 16 of the 44 samples were selected based on spatial distribution and the presence of illite for grain-size separation and for illite polytype analysis (these are indicated in data tables with an asterisk). Samples were crushed in an agate mortar and pestle, washed, and disaggregated in an ultrasonic bath. Sodium pyrophosphate was used as needed for deflocculation. Each sample was separated into five grain-sizes by centrifugation, using Stoke's Law. The resulting grain-sizes are as follows: very coarse (2-1 μm), coarse (1-0.5 μm), medium (0.1-0.5 μm), fine (0.05-.01 μm), and very fine (<0.05 μm). H isotopic analyses were conducted on each grain-size aliquot, and select samples were dated by $^{40}Ar/^{39}Ar$ geochronology.

4 Results and Analysis

4.1 X-ray Texture Goniometry

The results of 6 representative XTG analyses; 3 from the New York transect, 3 from the West Virginia transect show a common geographic trend (Figure 3). These pole figures are

This article is protected by copyright. All rights reserved.

arranged by geographic proximity to the orogenic belt. The illite crystallographic preferred orientation (CPO) fabric of all samples have symmetrical, circular patterns, which are characteristic for a post-sedimentation compaction fabric from diagenetic illite growing parallel to bedding (Day-Stirrat et al., 2008; Day-Stirrat et al., 2012). Minor elongation is detected in the samples closest to the orogen and indicate the presence of an incipient cleavage, but that component is weakly developed (Ho et al., 1999; Ho et al., 2001).

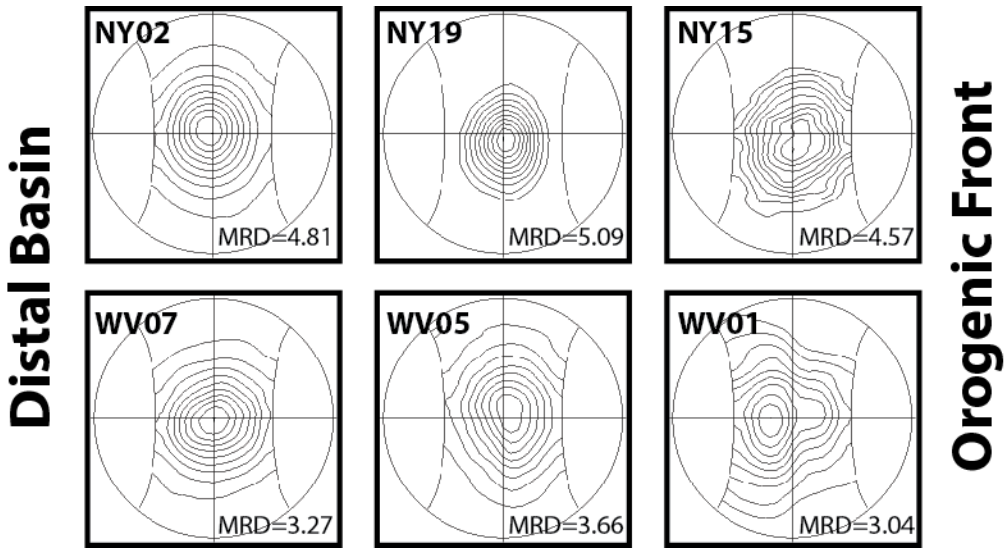

Figure 3 Pole-figure diagrams describing the CPO of illite in mudstone samples from two transects across the Appalachian basin. A single maximum in basinally distal rocks (NW) becomes elongated and eventually separates into two maxima, indicating the progressive growth of incipient cleavage when approaching the orogenic front (SW).

The MRD values expected for unconsolidated sediments at the time of deposition are 1.7-2.0 (Matenaar, 2002), ~6.0 at the onset of metamorphism (Day-Stirrat et al., 2008), and as high as ~12.0 for metamorphic pelites (Jacob et al., 2000). The values recorded in these samples, MRD 3-5, correspond to burial depths between 2-5 km (Ho et al., 1999; Day-Stirrat et al., 2010).

4.2 Illite Polytype Analysis

Q-XRPD results from Rietveld analysis of each of 5 size fractions for 16 sample sites are reported, with an error of ±2 weight percent (Table 1). The very fine size fractions of samples NY02 and PA01 were dominated by amorphous material, and illite polytypes could not be modeled using Q-XRPD. Robust model fits are achieved by BGMN ®, and the negative correlation between grain-size and the proportion of authigenic illite evident (Figure 4).

This article is protected by copyright. All rights reserved.

Author Manuscript

Author Manuscript

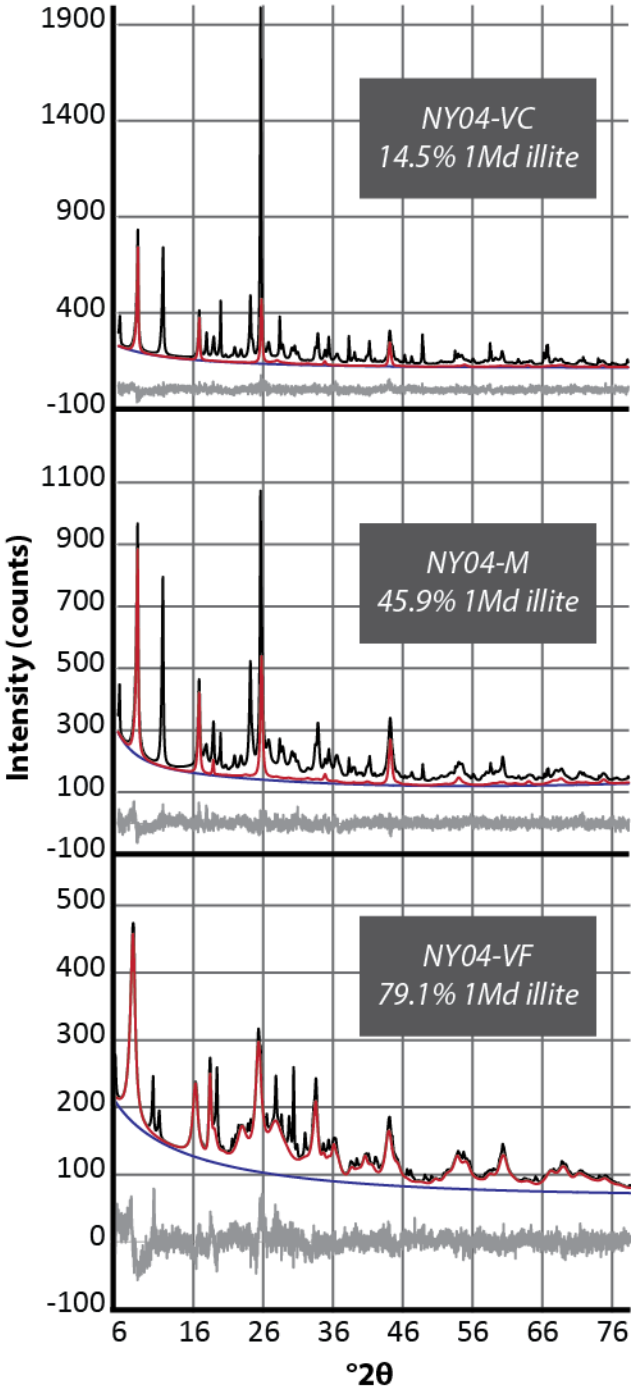

Figure 4 X-ray diffractograms of three grain-size fractions of sample NY04. Sample measurement data (black line), modeled 1Md illite (red line), calculated background (blue line), and difference between Rietveld model and measured spectrum (grey line) is displayed.

This article is protected by copyright. All rights reserved.

Author Manuscript

Table 1 Q-XRPD results (k=kaolinite, g=gypsum, d=dolomite, hb=hornblende, fl=fluorite, ap=apatite)

Sample ID	Quartz	1Md illite	2M1 illite	chlorite	calcite	K-feldspar	Plagioclase feldspar	Other
NY02-VC	11.03	49.10	10.87	18.60		1.95	8.52	
NY02-C	2.30	41.00	8.20	37.80		2.06	8.62	
NY02-M	1.88	50.80	7.97	26.00		3.01	10.31	
NY02-F		96.42	2.79	0.79				
NY04-VC	15.15	14.50	25.21	30.90	2.58			k=11.7
NY04-C	1.78	4.33	3.32	1.12	0.21			k=89.25
NY04-M	0.47	45.90	2.69	14.81	0.72			k=35.4
NY04-F	2.19	55.50	3.98	2.79				k=35.59
NY04-VF	0.46	79.10	1.98	1.81				k=16.7
NY07-VC	21.25	30.76	11.83	10.92	2.17		4.13	d=18.94
NY07-C	15.39	44.80	14.06	11.86	1.77		5.62	d=6.48
NY07-M	3.93	49.51	4.19	34.76	1.61		4.41	d=1.59
NY07-F	1.16	75.58	5.64	4.43	3.24		9.19	d=0.76
NY07-VF		89.11	2.74	4.66	3.49			
NY15-VC	17.43	51.60	10.53	6.36			14.11	
NY15-C	13.33	54.70	13.16	4.68			14.17	
NY15-M	3.19	65.60	8.86	22.30				
NY15-F		89.87	5.38	4.75				
NY15-VF		92.46	4.10	3.44				
NY19-VC	33.11	40.51	12.22	6.24	2.62	5.29		
NY19-C	26.92	49.98	10.43	6.51	1.58	4.58		
NY19-M	10.00	59.00	7.00	25.00				
NY19-F	3.56	87.27	4.10	5.06				
NY19-VF	1.11	87.92	2.93	1.45				g=6.59
OH02-VC	9.70	12.00	17.90			1.48		k=58.9

This article is protected by copyright. All rights reserved.

Author Manuscript

OH02-C	4.15	23.60	16.89	2.12		1.88		k=51.3
OH02-M		38.70	4.16					k=57.2
OH02-F		77.57	0.85					k=21.58
OH02-VF		93.88	3.83	2.29				
OH04-VC	8.10	13.80	30.22	2.43		2.86		k=42.7
OH04-C	4.28	30.20	1.94	4.00		5.26		k=54.3
OH04-M	13.50	40.00	11.70	12.00		15.80		k=7.3
OH04-F	2.20	83.30	3.39	4.10		6.51		
OH04-VF		85.00	4.81	5.38		4.82		
OH05-VC	21.00	14.30	12.90	5.54		4.84		k=41.4
OH05-C	4.10	16.90	4.96			2.02		k=72.1
OH05-M		9.00	3.06	3.92				k=84
OH05-F	0.06	57.30	2.15	7.10				k=33.4
OH05-VF		54.70	2.30	43.00				
PA01-VC	33.80	14.50	31.10	8.98	0.17	5.15		hb=5.12, fl=1.24
PA01-C	16.01	51.60	14.78	11.86		2.50		hb=2.92, fl=0.38
PA01-M	6.60	64.80	9.46	19.19				
PA01-F	0.80	88.43		4.97				ap=5.79
PA04-VC	14.80	6.36	23.33	4.38		2.78	0.72	k=47.6
PA04-C	3.45	11.30	10.57	8.76		0.39		k=65.5
PA04-M	2.16	11.80	5.27	1.82		1.55		k=77.4
PA04-F		48.00	3.00	49.00				
PA04-VF		91.69	4.79	3.52				
SNPA3-VC	32.63	30.80	18.89	10.57		1.32	5.78	
SNPA3-C	17.28	48.50	17.27	10.38		3.38	3.19	
SNPA3-M	5.41	63.30	14.39	7.36		2.58	6.97	
SNPA3-F	1.86	67.10	3.09	12.10		4.82	11.00	
SNPA3-VF	2.31	71.90	6.57	4.66		3.52	11.00	
SNPA7-VC	9.00	20.10	5.97	2.30				k=62.6
SNPA7-C	6.04	20.69	7.39	3.48				k=62.4

This article is protected by copyright. All rights reserved.

SNPA7-M	3.03	33.00	6.67	3.90				k=53.4
SNPA7-F	2.19	55.50	3.98	2.79				k=35.59
SNPA7-VF	0.64	43.30	2.27	2.39				k=51.4
SNPA8-VC	5.09	14.44	4.12			20.36		d=55.99
SNPA8-C	5.31	29.46	1.70			18.87		d=44.65
SNPA8-M	4.42	51.24	8.67			12.73		d=22.94
SNPA8-F	1.25	75.21	6.79			9.56		d=7.19
SNPA8-VF		89.69	4.89			4.04		d=1.39
WV01-VC	8.79	11.30	5.87	3.46	1.70	1.24	0.73	d=8.42, k=58.50
WV01-C	5.71	33.40	7.45	2.96	0.98			d=7.04, k=42.50
WV01-M	3.28	30.50	3.82	1.99				d=3.86, k=56.50
WV01-F	0.83	58.40	1.56	36.60	2.41			d=0.191
WV01-VF		93.02	3.64	3.34				
WV05-VC	11.96	3.81	18.30	3.06	0.06	0.90	1.75	d=0.10, k=60.10
WV05-C	2.85	7.70	3.40	1.37			1.24	k=83.4
WV05-M	2.93	5.26	12.06	1.99			7.41	k=70.4
WV05-F		88.81	4.17	5.77				
WV05-VF		93.51	3.43	3.06				
WV07-VC	10.84	5.33	20.96	4.99	1.92	2.09	0.99	d=1.19, k=51.70
WV07-C	6.38	15.60	24.31	2.75	1.41	0.78		d=0.88, k=47.90
WV07-M	2.49	7.99	13.21	2.29	1.48	1.33	5.11	d=0.64, k=65.50
WV07-F	0.15	30.00	1.89	3.76	2.15	1.24		d=0.58, k=60.30
WV07-VF		68.10	3.46	3.62				k=24.8

4.3 Hydrogen Isotopes

The results of H isotopic analysis of each of the 5 size fractions for 16 selected samples are reported in Table 2. The data exhibit high repeatability and generally show positive correlation with grain size. Using the measured H isotopic compositions and Q-XRPD results of each grain-size, mixing plots are created for those samples located within the Appalachian Plateau (Figure 5). This excludes samples SNPA3, SNPA7, and SNPA8, which were collected in

This article is protected by copyright. All rights reserved.

Author Manuscript

the Valley and Ridge province. The anomalously low value in sample PA01-VF is attributed to the presence of organic material or apatite, and, because the size fraction cannot be modeled by Q-XRPD, it is not used to calculate the mixing line for that sample. The extrapolated authigenic (1Md) clay end-member values and the extrapolated high-T hydrous mineral aggregate end-member values, after York regression analysis, are reported in Table 3.

Table 2 H Isotopic Results

Sample ID	δD	δD (repeat)	Sample ID	δD	δD (repeat)
NY02-VC	-79	-79	PA01-VC	-77	-75
NY02-C	-79		PA01-C	-76	-76
NY02-M	-81		PA01-M	-74	-73
NY02-F	-87	-89	PA01-F	-91	
NY02-VF	-104		PA01-VF	-121	
NY04-VC	-66	-69	PA04-VC	-62	-64
NY04-C	-68	-70	PA04-C	-65	
NY04-M	-73	-72	PA04-M	-68	-68
NY04-F	-75	-73	PA04-F	-77	
NY04-VF	-77	-78	PA04-VF	-82	
NY07-VC	-71	-70	SNPA3-VC	-70	
NY07-C	-73	-73	SNPA3-C	-70	-67
NY07-M	-78		SNPA3-M	-74	
NY07-F	-78	-76	SNPA3-F	-83	
NY07-VF	-78		SNPA3-VF	-76	
NY15-VC	-70	-69	SNPA7-VC	-69	-70
NY15-C	-70	-70	SNPA7-C	-69	-69
NY15-M	-70	-68	SNPA7-M	-74	-73
NY15-F	-74	-71	SNPA7-F	-83	-81
NY15-VF	-73	-74	SNPA7-VF	-76	-74
NY19-VC	-71	-73	SNPA8-VC	-72	-72

Author Manuscript

This article is protected by copyright. All rights reserved.

NY19-C	-72	-70	SNPA8-C	-77	-74
NY19-M	-75	-74	SNPA8-M	-75	-76
NY19-F	-78	-78	SNPA8-F	-84	-81
NY19-VF	-75		SNPA8-VF	-76	-78
OH02-VC	-57	-54	WV01-VC	-60	-63
OH02-C	-58	-58	WV01-C	-60	-63
OH02-M	-63	-61	WV01-M	-64	-64
OH02-F	-77		WV01-F	-72	-68
OH02-VF	-82		WV01-VF	-75	-74
OH04-VC	-56	-56	WV05-VC	-61	-62
OH04-C	-54	-55	WV05-C	-62	-62
OH04-M	-63	-62	WV05-M	-64	-62
OH04-F	-76	-73	WV05-F	-73	-72
OH04-VF	-83		WV05-VF	-75	-73
OH05-VC	-62	-61	WV07-VC	-51	-49
OH05-C	-59	-59	WV07-C	-50	-48
OH05-M	-61	-60	WV07-M	-54	-53
OH05-F	-69	-72	WV07-F	-63	
OH05-VF	-72	-70	WV07-VF	-66	

Author Manuscript

This article is protected by copyright. All rights reserved.

Author Manuscript

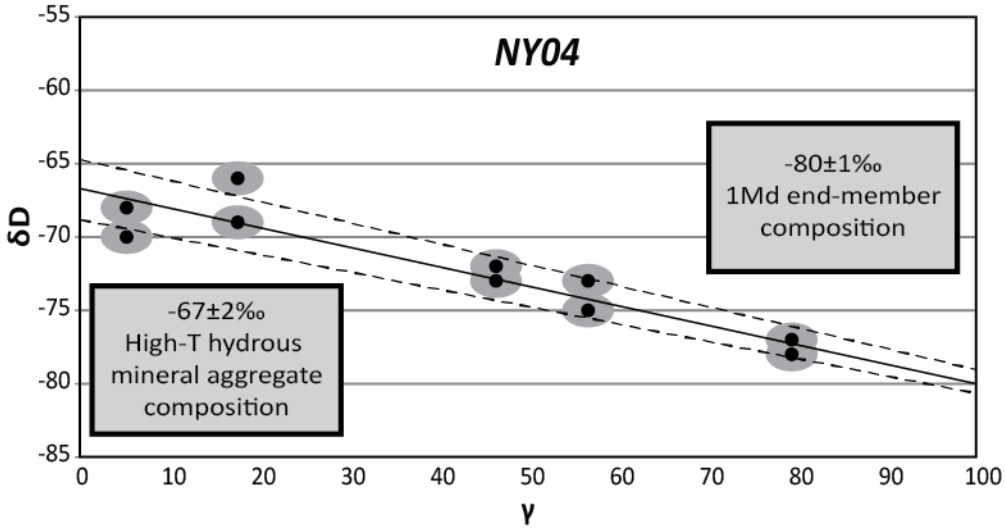

Figure 5 Mixing line with York-type linear regression analysis between H isotopic composition and abundance of authigenic illite (γ is defined in equation 1 of the text). Uncertainty is indicated by grey spheres and dashed lines. Extrapolated end-member isotopic compositions for 1Md illite and a chlorite-dominated high-T hydrous clay mineral aggregate are displayed.

Table 3 Extrapolated end-member and calculated fluid δD results

Sample ID	δD 1Md illite (‰)	δD 1Md mineralizing fluid (‰)	Fractionation Temperature (°C)	δD chlorite (‰)	δD chlorite mineralizing fluid (‰)
NY02	-88	-55	80	-67	-37
NY04	-80	-50	90	-67	-37
NY07	-79	-52	100	-64	-34
NY15	-75	-72	190	-56	-25
NY19	-78	-57	120	-61	-31
OH02	-84	-57	100	-50	-19
OH04	-88	-58	90	-44	-14
OH05	-82	-48	80	-57	-26
PA01	-89	-59	90	-60	-30
PA04	-86	-62	110	-63	-33
WV01	-76	-61	140	-57	-27
WV05	-74	-57	130	-61	-31
WV07	-78	-54	110	-48	-18

This article is protected by copyright. All rights reserved.

Author Manuscript

In order to convert the end-member isotopic values to equilibrium fluid compositions, constraints on the temperature of crystallization are needed. Figure 6 overlays the sample locations onto the conodont alteration index map of Harris (1979), and indicates the fractionation temperature utilized and equilibrium fluid value for both end-members of each of the samples (Table 3).

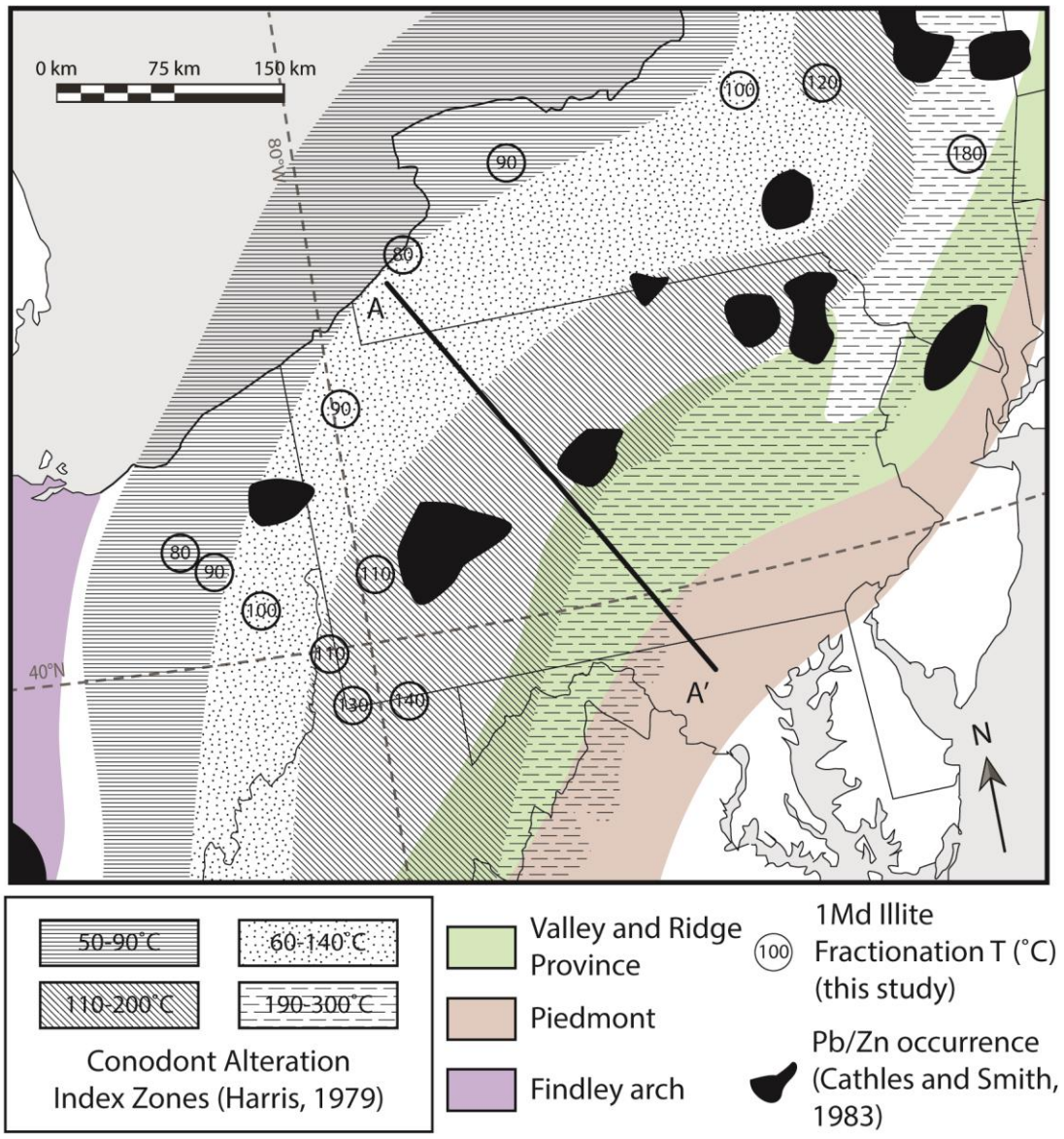

Figure 6 Map of study area, overlaying select Appalachian Plateau samples onto the Ordovician carbonate rock conodont alteration zones of Harris (1979). The numbers in the sample location circles indicate the chosen formation temperature utilized in H isotopic fractionation calculations. A-A' is the cross-section line in Figure 8.

This article is protected by copyright. All rights reserved.

Author Manuscript

4.4 $^{40}Ar/^{39}Ar$ Geochronology

Table 4 1Md:2M1 illite ratio and total gas age for each of the dated size fractions. Sample ages were calibrated with standards and reruns after an initial flow-line leak affected the first set.

Sample	1Md (%)	2M1 (%)	1Md/(1Md+2M1)*100	2M1/(1Md+2M1)*100	Total Gas Age (Ma)	1σ Error (±Ma)
NY04_VC	14.50	25.21	36.51	63.49	408.65	1.745
NY04_C	4.33	3.32	56.60	43.40	403.855	1.689
NY04_F	55.50	3.98	93.31	6.69	344.981	1.333
NY04_VF	79.10	1.98	97.56	2.44	302.223	1.358
NY07_VC	30.76	11.83	72.22	27.78	438.178	2.224
NY07_C	44.80	14.06	76.11	23.89	430.69	1.44
NY07_F	75.58	5.64	93.06	6.94	344.027	1.104
NY07_VF	89.11	2.74	97.02	2.98	319.975	1.182
NY15_C	54.70	13.16	80.61	19.39	441.623	2.09
NY15_M	65.60	8.86	88.10	11.90	375.674	1.342
NY15_F	89.87	5.38	94.35	5.65	365.452	1.32
NY15_VF	92.46	4.10	95.75	4.25	335.53	1.517
NY19_C	49.98	10.43	82.73	17.27	485.52	2.311
NY19_M	59.00	7.00	89.39	10.61	422.355	1.285
NY19_F	87.27	4.10	95.51	4.49	352.148	1.22
NY19_VF	87.92	2.93	96.77	3.23	250.236	1.404

Samples NY04, NY07, NY15, and NY19 were selected for Ar dating in order to create a representative transect across the Appalachian Plateau (Table 4). Sample NY19-VF exhibited extreme Cl/K ratios during degassing (indicative of non-clay crystalline phases such as zeolite, or high organic content) and was excluded from age analysis. Age analysis calculates an end-member 1Md illite formation age of 317.7±3.4 Ma and a 2M1 illite formation age of 483.4±11.5 Ma for sample NY04; a 1Md illite formation age of 309.9±10.3 Ma and a 2M1 illite formation age of 723.4±51.9 Ma for sample NY07; a 1Md illite formation age of 309.1±18.8 Ma and a 2M1 illite formation age of 923.5±127.7 Ma for sample NY15; and a 1Md illite formation age of

This article is protected by copyright. All rights reserved.

Author Manuscript

308.1±35.4 Ma and a 2M1 illite formation age of 1161.2±208.2 Ma for sample NY19 (figure 7). Due to the limited range of 1Md:2M1 ratios exhibited by samples NY07, NY15, and NY19, the large uncertainty estimates reported from the regression analysis are dominated by the unochron error (an effect of a much smaller range in %1Md than the range in age), although the high proportions of 1Md illite in the finest-grained samples gives high confidence to the calculated end-member 1Md illite age (van der Pluijm and Hall, 2015).

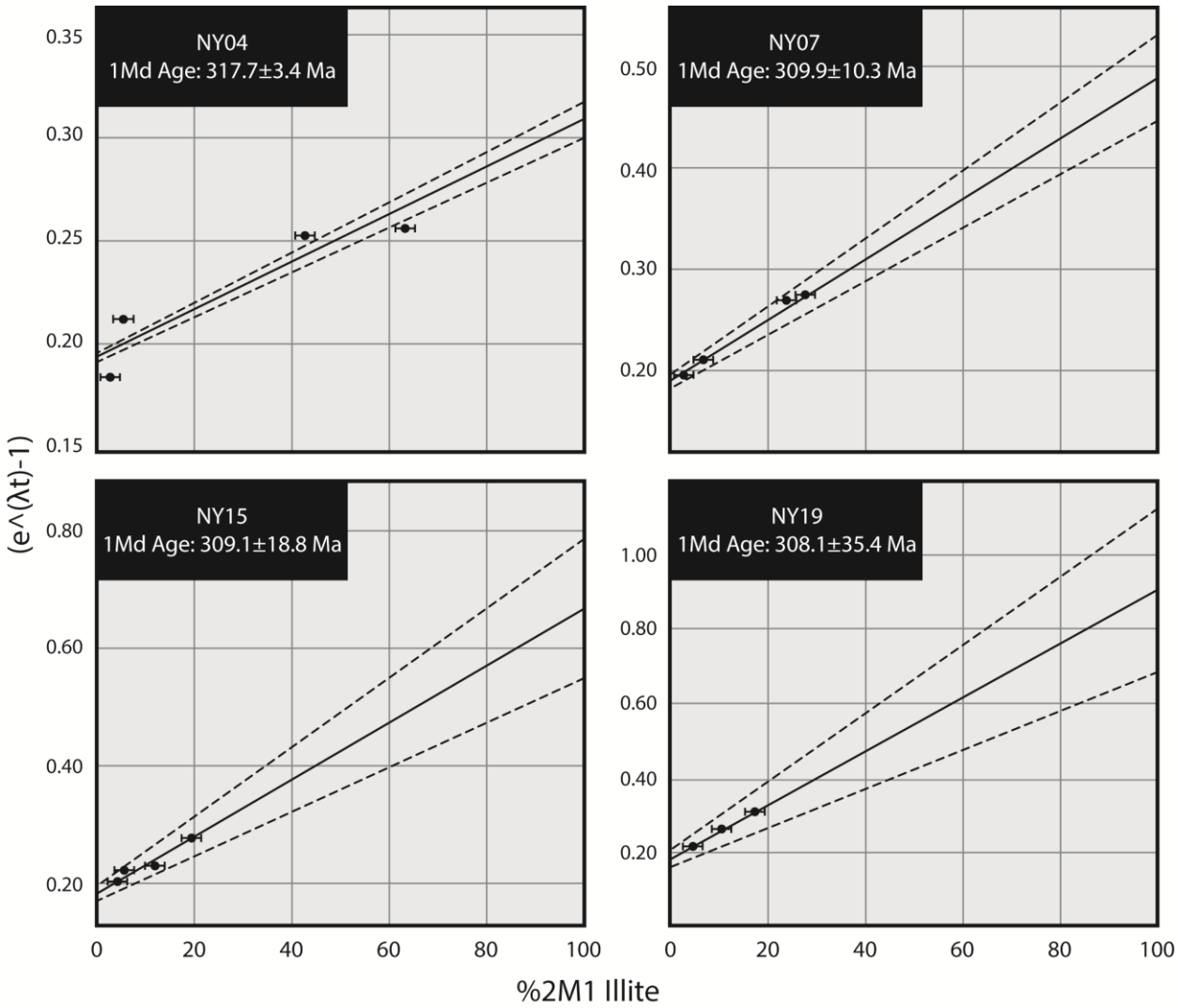

Figure 7 Age analysis of samples NY04, NY07, NY15, and NY19.

5 Discussion

To examine the geographic variability of the mineralizing fluid compositions, the data is projected onto a composite cross section line A-A' (from figure 6) with distance from the Appalachian orogenic front (figure 8). In this generalized section, a negative correlation between

This article is protected by copyright. All rights reserved.

Author Manuscript

1Md illite δD composition and geographic proximity to the orogenic front is observed; samples located further into the craton display more negative 1Md illite compositions. However, when paired with the understanding that a sampling transect from the modern day surface of the Appalachian Plateau represents rocks that occupied increasingly deeper stratigraphic levels and higher diagenetic grades (and thus higher formation temperatures) towards the orogen, the mineralizing fluid compositions display a positive correlation with geographic proximity to the orogenic front. This pattern is predicted by clay-fluid H isotopic partitioning that yields higher and more deuterium-enriched fractionations at lower temperatures.

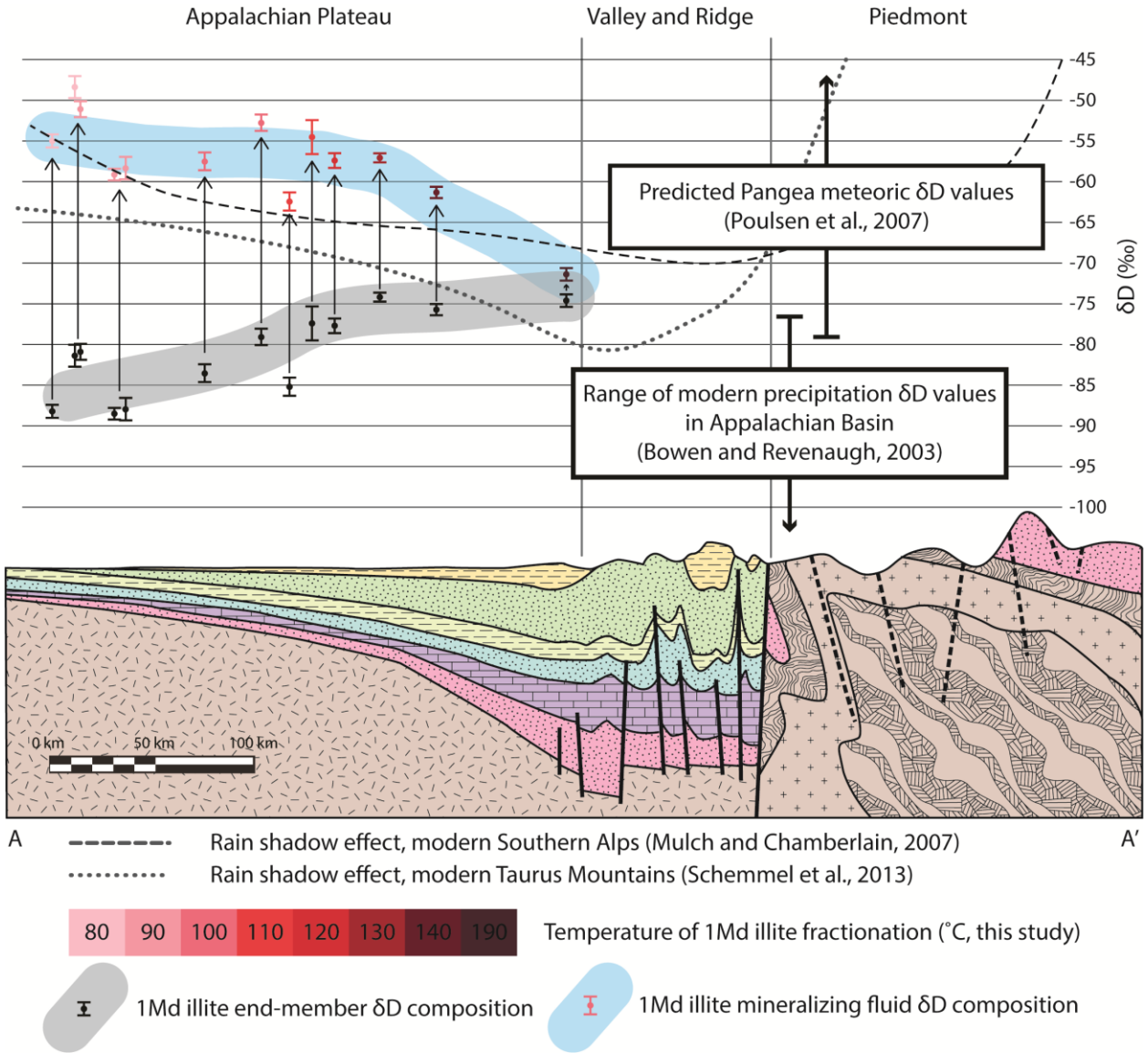

Figure 8 Composite idealized cross-section of the central Appalachian Plateau and orogen. Both crystalline phase and equilibrium fluid compositions are displayed, color coded by utilized fractionation temperature. δD ranges of modeled late Paleozoic meteoric fluid and modern Appalachian basin meteoric fluid are displayed, as are rain shadow trends from modern orogens (geology from Cleaves et al., 1968; Ryder et al., 2009).

This article is protected by copyright. All rights reserved.

Author Manuscript

Depositional geothermal gradient estimates in the Appalachian basin are 25-30ºC/km (Reed et al., 2005), so at formation temperatures of 80-190ºC, diagenesis and 1Md illite neoformation occurred at depths of 3-6 km. Estimates of erosion from the Appalachian Plateau, based on coal rank, conodont alteration index, critical wedge theory, apatite fission track analysis, and Atlantic-margin sediment volume calculations, postulate 2-9 km of denuded topography, which accounts for the decreasing temperature away from the orogen (Mathews, 1975; Friedman and Sanders, 1978; Slingerland and Furlong, 1989; Blackmer et al., 1994; Reed et al., 2005).

Beyond the trend with distance, the calculated mineralizing fluid compositions are less negative than the range of modern precipitation in the Appalachian basin, which is fully consistent with the southerly paleogeographic latitude of North America in Pangea reconstructions and elevated mean surface temperatures during that time (Vander Voo, 1988; Peyser and Poulsen, 2008; Bowen and Revenaugh, 2003; Torsvik et al., 2002). The mineralizing fluid compositions of illite match the range and trend of modeled Pangea meteoric fluid values (using $\delta D \approx 8 * \delta^{18}O$; Poulsen et al., 2007). The geographic-dependent results are consistent with a rain shadow effect that is observed in modern day orogenic belts, such as the Taurus Mountains and the Southern Alps (Mulch and Chamberlain, 2007; Schemmel et al., 2013).

The isotopic memory of the clay minerals in the Appalachian basin shows i) that equilibrium fluid facilitating diagenesis and 1Md illite neomineralization was surface-derived (meteoric), ii) that fluid was locally sourced on spatial scales small enough to preserve a rain shadow effect, and iii) that a mechanism for deep infiltration of surface fluid to depths of 3-6 km was involved. These depths of infiltration are sufficient to heat the fluids to temperatures suitable for 1Md illite growth and explain the occurrence of enigmatic high-temperature fluids at distal basin margins.

The high-T aggregate isotopic composition of the samples has no geographic trend and occupies a narrow range of values with an average value of -55‰. The average high-T fluid composition of all 16 samples is -25‰, well within the predicted metamorphic fluid range (Sheppard, 1986; Schedl et al., 1993). Their narrow range of values within the metamorphic field confirms that high temperature clays are detrital and reflecting the composition of their orogenic

This article is protected by copyright. All rights reserved.

provenance. The rock fabric of K-metasomatic illite from the XTG data shows burial compaction textures forming at depths between 2-5 km.

The timing of diagenetic 1Md illite neoformation, as obtained from age analysis, has a well-defined late Carboniferous range of 318-308 Ma. These ages corroborate previous studies that link the timing of K-alteration in the North American midcontinent with Alleghanian orogenesis (320-270 Ma; (Schedl et al., 1993; Elliott and Aronson, 1987; Hay et al., 1988; Hearn et al., 1987; Clauer et al., 2013). The timing of 1Md illite mineralization recorded in this study also coincides with regional MVT formation. Leach et al. (2001) review MVT deposit timing of 400-260 Ma and 180-40 Ma from various radiometric and paleomagnetic techniques. The Carboniferous ages are contemporary with Alleghanian oroclinal bending during the Kiaman Reverse Superchron (Cederquist, 2006) and slightly predate Valley and Ridge Province folding, estimated by Stamatakos et al. (1996) with a mean age of ~267 Ma. Figure 9 places illite mineralization ages in the tectonic context of eastern North America and shows no spatio-temporal trend associated with diagenesis, which would be predicted from a westward-driven, time-dependent regional fluid flow scenario. Instead, surface-fluid derived diagenesis occurred in the same time range and across the whole of the Appalachian Plateau. We surmise that the systematic and pervasive joint sets that formed in the Appalachian Plateau from burial and far-field stress transmission during Alleghanian deformation (Nickelsen and Hough, 1967; Engelder, 1985; Engelder et al., 2009; Engelder and Lacazette, 1990; Jacobi, 2002) provided ubiquitous fluid pathways for locally sourced surface fluid infiltration to several km depths.

Author Manuscript

This article is protected by copyright. All rights reserved.

Author Manuscript

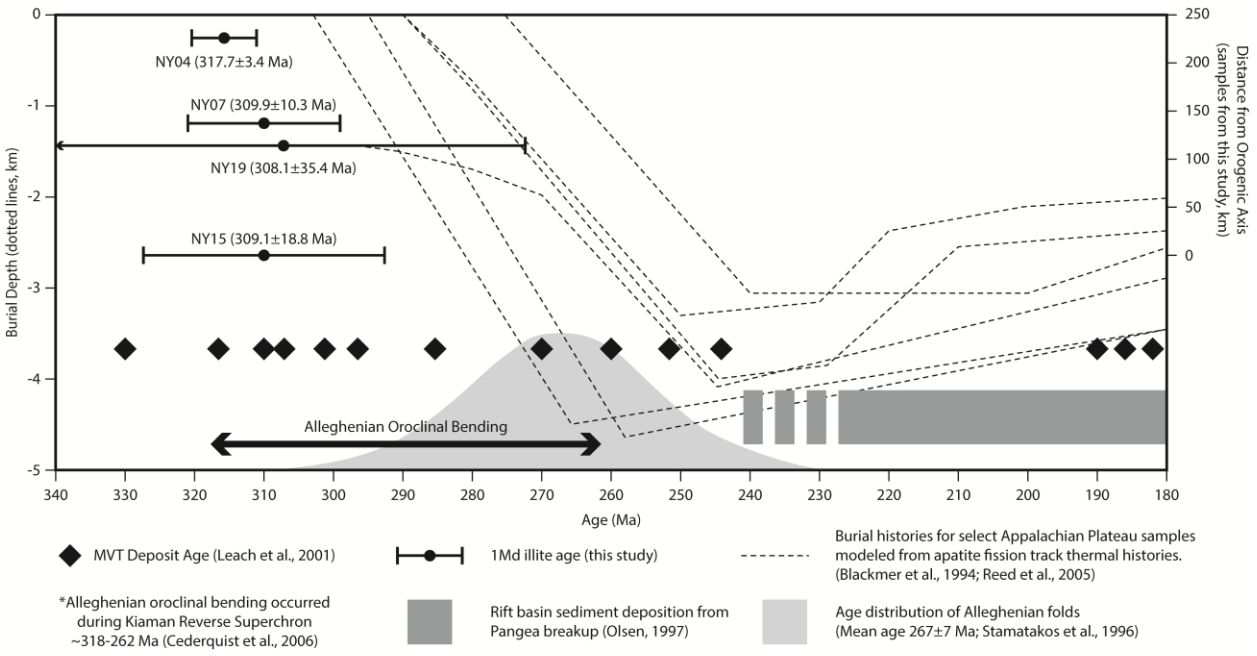

Figure 9 Diagenetic ages are plotted in context of the tectonic activity in the Appalachian Plateau. The ages are compared to apatite fission track analysis, Alleghanian oroclinal rotation fold timing, and Pangea break-up synrift strata deposition timing. The ages correspond to the onset of Alleghanian regional stress transmission.

6 Conclusions

The pairing of H isotopic analysis and Ar radiometric dating of authigenic clays in the sedimentary cover rocks of the Appalachian Plateau provides a powerful tool to constrain the regional conditions and relationships between diagenesis and orogeny. 1Md illite authigenesis occurred at temperatures between 80-190ºC and at depths of 3-6 km, from a mineralizing fluid that was predominantly surface-derived (meteoric). The timing of clay diagenesis is coeval with the Alleghanian orogenic pulse of the Appalachians in this part of the orogen. The surface fluid source was sufficiently localized to preserve a rain shadow effect from the high elevation Appalachian orogen.

We find no evidence in authigenic illite of the Appalachian Plateau for long-distance, metamorphic fluid migration, challenging the popular hypothesis of orogenic fluid expulsion for regional mineralization and remagnetization. Instead, we posit that Alleghanian far-field stresses within the foreland sequence provided the driving force for abundant fluid infiltration into the upper crust.

This article is protected by copyright. All rights reserved.

Author Manuscript

Acknowledgments, Samples, and Data

We thank Andreas Mulch for H isotopic analysis, Chris Hall for Ar dating, and Samantha Nemkin for preliminary sampling in the Valley and Ridge Province of Pennsylvania. We thank the Sedimentary Geology Division and Structural Geology and Tectonics Division of the Geological Society of America for the Stephen E. Laubach Research in Structural Diagenesis Award, and the Clay Minerals Society for the Robert C. Reynolds, Jr. Research Award that supported this research. Our work on Appalachian clay mineralization is supported by the National Science Foundation under EAR-1629805. This manuscript benefitted greatly from Bob Hatcher and an additional anonymous reviewer. The data used in this work are listed in the references, text, tables, and figures in the manuscript. Unrestricted access to sample location data and descriptions is available online using the SESAR (System for Earth Sample Registration) repository, with IGSN's (International Geo Sample Numbers) listed in figure 1 (http://www.geosamples.org/). Radiogenic dating, stable isotopic dating, and quantitative X-ray powder diffraction results are publicly available in the University of Michigan's Deep Blue data repository (https://doi.org/10.7302/7knb-kf94).

References

Bachu, S., 1995, Synthesis and model of formation-water flow, Alberta Basin, Canada: American Association of Petroleum Geologists Bulletin, v. 79, no. 8, p. 1159–1178, doi: 10.1306/8D2B2209-171E-11D7-8645000102C1865D.

Bergmann, J., Friedel, P., and Kleeberg, R., 1998, BGMN—a new fundamental parameter based Rietveld program for laboratory X-ray sources, its use in quantitative analysis and structure investigations: Commission of Powder Diffraction, p. 5–8.

Bethke, C., 1986, Hydrologic constraints on the genesis of the Upper Mississippi Valley mineral district from Illinois basin brines: Economic Geology, v. 81.

Bethke, C., and Marshak, S., 1990, Brine migrations across North America-the plate tectonics of groundwater: Annual Review of Earth and Planetary Sciences, no. 18, p. 287–315.

Bjorlykke, K., 1994, Fluid-flow processes and diagenesis in sedimentary basins: Geological Society, London, Special Publications, v. 78, no. 1, p. 127–140, doi: 10.1144/GSL.SP.1994.078.01.11.

This article is protected by copyright. All rights reserved.

Author Manuscript

Bjorlykke, K., 1993, Fluid flow in sedimentary basins: Sedimentary Geology, v. 86, no. 1–2, p. 137–158, doi: 10.1016/0037-0738(93)90137-T.

Blackmer, G.C., Omar, G.I., and Gold, D.P., 1994, Post-Alleghanian unroofing history of the Appalachian Basin, Pennsylvania, from fission track analysis and thermal models: Tectonics, v. 13, no. 5, p. 1259–1276.

Boles, A., Schleicher, A. M., Solum, J., and van der Pluijm, B., 2018, Quantitative X-ray powder diffraction and the illite polytype analysis method for direct fault rock dating: A comparison of analyitical techniques: Clays and Clay Minerals, v. 66, no. 3, pp. 220-232(13), doi: https://doi.org/10.1346/CCMN.2018.064093

Boles, A., van der Pluijm, B., Mulch, A., Mutlu, H., Uysal, I.T., and Warr, L.N., 2015, Hydrogen and 40Ar/39Ar isotope evidence for multiple and protracted paleofluid flow events within the long-lived North Anatolian Keirogen (Turkey): Geochemistry Geophysics Geosystems, p. 1541–1576, doi: 10.1002/2014GC005684.Key.

Bowen, G.J., and Revenaugh, J., 2003, Interpolating the isotopic composition of modern meteoric precipitation: Water Resources Research, v. 39, no. 10, p. n/a-n/a, doi: 10.1029/2003WR002086.

Bull, J.M., 1990, Structural style of intra-plate deformation, Central Indian Ocean Basin: evidence for the role of fracture zones: Tectonophysics, v. 184, no. 2, p. 213–228, doi: 10.1016/0040-1951(90)90054-C.

Buyce, M., and Friedman, G., 1975, Significance of authigenic K-feldspar in Cambrian-Ordovician carbonate rocks of the proto-Atlantic shelf in North America: Journal of Sedimentary Research, v. 45, no. 4, p. 808–821.

Capuano, R., 1992, The temperature dependence of hydrogen isotope fractionation between clay minerals and water: Evidence from a geopressured system: Geochimica et Cosmochimica Acta, v. 56, no. 6, p. 2547-2554.

Carlson, E.H., 1994, Geologic, Fluid Inclusion, and Isotopic Studies of the Findlay Arch District, Northwestern Ohio: Economic Geology, v. 89, p. 67–90.

Cathles, L.M., and Smith, A.T., 1983, Thermal constraints on the formation of Mississippi Valley-type lead- zinc deposits and their implications for episodic basin dewatering and

This article is protected by copyright. All rights reserved.

Author Manuscript

deposit genesis.: Economic Geology, v. 78, no. 5, p. 983–1002, doi: 10.2113/gsecongeo.78.5.983.

Cederquist, D.P., Vander Voo, R., van der Pluijm, B.A., 2006, Syn-folding remagnetization of Cambro-Ordovician carbonates from the Pennsylvania Salient post-dates oroclinal rotation: Tectonics, no. 422, pp. 41-54, doi:10.1016/j.tecto.2006.05.005

Clauer, N., Fallick, A., and Eberl, D., 2013, K-Ar dating and δ18O-δD characterization of nanometric illite from Ordovician K-bentonites of the Appalachians: Illitization and the Acadian-Alleghenian tectonic activity: American Mineralogist, v. 98, no. 11-12, p. 2144–2154.

Clayton, J.L., and Swetland, P.J., 1980, Petroleum Generation and Migration in Denver Basin: AAPG Bulletin, v. 64, no. 10, p. 1613–1633, doi: 10.1306/C1EA57CE-16C9-11D7-8645000102C1865D.

Cleaves, E.T., Edwards, J.J., Glaser, J.D., and Weaver, K.N., 1968, Geologic Map of Maryland: Geologic Map, Maryland Geological Survey, v. 2 sheets.

Craddock, J., Jackson, M., van der Pluijm, B., and Versical, R., 1993, Regional shortening fabrics in eatern North America: far-field stress transmission from the Appalachian-Ouachita orogenic belt: Tectonics, v. 12, no. 1, p. 257–264.

Day-Stirrat, R.J., Aplin, A.C., Środoń, J., and van der Pluijm, B. A., 2008, Diagenetic Reorientation of Phyllosilicate Minerals in Paleogene Mudstones of the Podhale Basin, Southern Poland: Clays and Clay Minerals, v. 56, no. 1, p. 100–111, doi: 10.1346/CCMN.2008.0560109.

Day-Stirrat, R.J., Dutton, S.P., Milliken, K.L., Loucks, R.G., Aplin, A.C., Hillier, S., and van der Pluijm, B. A., 2010, Fabric anisotropy induced by primary depositional variations in the silt: clay ratio in two fine-grained slope fan complexes: Texas Gulf Coast and northern North Sea: Sedimentary Geology, v. 226, no. 1–4, p. 42–53, doi: 10.1016/j.sedgeo.2010.02.007.

Day-Stirrat, R.J., Flemings, P.B., You, Y., Aplin, A.C., and van der Pluijm, B. A., 2012, The fabric of consolidation in Gulf of Mexico mudstones: Marine Geology, v. 295–298, p. 77–85, doi: 10.1016/j.margeo.2011.12.003.

This article is protected by copyright. All rights reserved.

Author Manuscript

Day-Stirrat, R.J., Loucks, R.G., Milliken, K.L., Hillier, S., and van der Pluijm, B.A., 2008, Phyllosilicate orientation demonstrates early timing of compactional stabilization in calcite-cemented concretions in the Barnett Shale (Late Mississippian), Fort Worth Basin, Texas (U.S.A): Sedimentary Geology, v. 208, no. 1–2, p. 27–35, doi: 10.1016/j.sedgeo.2008.04.007.

Deming, D., and Nunn, J.A., 1991, Numerical simulations of brine migration by topographically driven recharge: Journal of Geophysical Research, v. 96, no. B2, p. 2485–2499.

Deming, D., Nunn, J. A., and Evans, D.G., 1990, Thermal effects of compaction-driven groundwater flow from overthrust belts: Journal of Geophysical Research, v. 95, no. b5, p. 6669, doi: 10.1029/JB095iB05p06669.

Elliott, W.C., and Aronson, J.L., 1987, Alleghanian episode of K-bentonite illitization in the southern Appalachian Basin: Geology, v. 15 n. 8, p. 735, doi: 10.1130/0091-7613(1987)15<735.

Engelder, T., 1985, Loading paths to joint propagation during a tectonic cycle: an example from the Appalachian Plateau, U.S.A.: Journal of Structural Geology, v. 7, no. 3–4, p. 459–476, doi: 10.1016/0191-8141(85)90049-5.

Engelder, T., and Lacazette, A., 1990, Natural Hydraulic Fracturing: Rock Joints, p. 35–44.

Engelder, T., Lash, G.G., and Uzcátegui, R.S., 2009, Joint sets that enhance production from Middle and Upper Devonian gas shales of the Appalachian Basin: AAPG Bulletin, v. 93, no. 7, p. 857–889, doi: 10.1306/03230908032.

Fitz-Díaz, E., Hall, C., and van der Pluijm, B., 2016, XRD-based 40Ar/39Ar age correction for fine-grained illite, with application to folded carbonates in the Monterrey Salient (northern Mexico): Geochimica et Cosmochimica Acta, doi: 10.1016/j.gca.2016.02.004.

Fitz-Diaz, E., Hudleston, P., Siebenaller, L., Kirschner, D., Camprubí, A., Tolson, G., and Puig, T.P., 2011, Insights into fluid flow and water-rock interaction during deformation of carbonate sequences in the Mexican fold-thrust belt: Journal of Structural Geology, v. 33, no. 8, p. 1237–1253, doi: 10.1016/j.jsg.2011.05.009.

Friedman, G.M., and Sanders, J.E., 1978, Time-temperature-burial significance of Devonian anthracite implies former great (6.5 km) depth of burial of Catskill Mountains, New

This article is protected by copyright. All rights reserved.

Author Manuscript

York: Geology, v. 10, n. 2, p. 93, doi: 10.1130/0091-7613(1982)10<93:TSODAI>2.0.CO;2.

Garven, G., 1995, Continental-scale groundwater flow and geologic processes: Annual Review of Earth and Planetary Sciences, v. 23, p. 89–117.

Graham, C.M., Viglino, J. A., and Harmon, R.S., 1987, Experimental study of hydrogen-isotope exchange between aluminous chlorite and water and of hydrogen diffusion in chlorite: American Mineralogist, v. 72, p. 566–579.

Grathoff, G.H., Moore, D.M., Hay, R.L., and Wemmer, K., 2001, Origin of illite in the lower Paleozoic of the Illinois basin: Evidence for brine migrations: Geological Society of America Bulletin, v. 113, no. 8, p. 1092–1104, doi: 10.1130/0016-7606(2001)113<1092:OOIITL>2.0.CO;2.

Hall, C.M., 2013, Direct measurement of recoil effects on 40Ar/39Ar standards, in Jourdan, F., Mark, D.F., and Verati, C. eds., Advances in 40Ar/39Ar Dating: from Archaeology to Planetary Sciences, Geological Society, London, Special Publications.

Harris, A.G., 1979, Conodont color alteration, an organo-mineral metamorphic index and its application to Appalachian Basin geology: Geology, no. 26, p. 3–16.

Hatcher, R., 2010, The Appalachian orogen: A brief summary: Geological Society of America Memoir, v. 206, no. 1, p. 1–19, doi: 10.1130/2010.1206(01).

Hay, R.L., Lee, M., Kolata, D.R., Matthews, J.C., and Morton, J.P., 1988, Episodic potassic diagenesis of Ordovician tuffs in the Mississippi Valley area: Geology, v. 16, no. 8, p. 743, doi: 10.1130/0091-7613(1988)016<0743:EPDOOT>2.3.CO;2.

Hearn, P., Sutter, J., and Belkin, H., 1987, Evidence for Late-Paleozoic brine migration in Cambrian carbonate rocks of the central and southern Appalachians: Implications for Mississippi Valley-type sulfide mineralization: Geochimica et Cosmochimica Acta, v. 51, p. 1323–1334.

Hnat, J.S., and van der Pluijm, B. a., 2014, Fault gouge dating in the Southern Appalachians, USA: Geological Society of America Bulletin, , no. February, doi: 10.1130/B30905.1.

This article is protected by copyright. All rights reserved.

Author Manuscript

Ho, N.C., Peacor, D.R., and van der Pluijm, B.A., 1995, Reorientation mechanisms of phyllosilicates in the mudstone-to-slate transition at Lehigh Gap, Pennsylvania: Journal of Structural Geology, v. 17, no. 3, p. 345–356, doi: 10.1016/0191-8141(94)00065-8.

Ho, N.C., Peacor, D.R., and van der Pluijm, B.A., 1999, Preferred orientation of phyllosilicates in Gulf Coast mudstones and relation to the smectite-illite transition: Clays and Clay Minerals, v. 47, no. 4, p. 495–504, doi: 10.1346/CCMN.1999.0470412.

Ho, N.C., van der Pluijm, B.A., and Peacor, D.R., 2001, Static recrystallization and preferred orientation of phyllosilicates: Michigamme Formation, Northern Michigan, USA: Journal of Structural Geology, v. 23, no. 6–7, p. 887–893, doi: 10.1016/S0191-8141(00)00162-0.

Jacob, G., Kisch, H.J., and van der Pluijm, B.A., 2000, The relationship of phyllosilicate orientation, X-ray diffraction intensity ratios, and c/b fissility ratios in metasedimentary rocks of the Helvetic zone of the Swiss Alps and the Caledonides of Jamtland, central western Sweden: Journal of Structural Geology, v. 22, no. 2, p. 245–258, doi: 10.1016/S0191-8141(99)00149-2.

Jacobi, Robert D., 2002, Basement faults and seismicity in the Appalachian Basin of New York State, in Neotectonics and Seismicity in the Eastern Great Lakes Basin, R. H. Fakundiny, R. D. Jacobi, and C. F. M. Lewis (eds.): Tectonophysics, v. 353, p.75-113.

Kleeberg, R., 2009, State-of-the-art and trends in quantitative phase analysis of geological and raw materials: European Powder Diffraction Conference, v. 30, p. 47–52, doi: 10.1524/zksu.2009.0007.

Knipe, R.J., and McCaig, a. M., 1994, Microstructural and microchemical consequences of fluid flow in deforming rocks: Geological Society, London, Special Publications, v. 78, no. 1, p. 99–111, doi: 10.1144/GSL.SP.1994.078.01.09.

Leach, D.L., Bradley, D., Lewchuk, M.T., Symons, D.T.A., De Marsily, G., and Brannon, J., 2001, Mississippi Valley-type lead-zinc deposits through geological time: Implications from recent age-dating research: Mineralium Deposita, v. 36, no. 8, p. 711–740, doi: 10.1007/s001260100208.

This article is protected by copyright. All rights reserved.

Author Manuscript

Lu, G., Mccabe, C., Hanor, J.S., and Ferrell, R.E., 1991, A genetic link between remagnetization and potassic metasomatism in the Devonian Onondaga Formation, Northern Appalachian Basin: Geophysical Research Letters, v. 18, no. 11, p. 2047–2050.

Mahon, K., 1996, The New "York" regression: Application of an improved statistical method to geochemistry: International Geology Review, v. 38, p. 293–303.

Manning, E.B., and Elmore, R.D., 2012, Rock magnetism and identification of remanence components in the Marcellus Shale, Pennsylvania: Geological Society, London, Special Publications, v. 371, no. 1, p. 271–282, doi: 10.1144/SP371.9.

Marshak, S., Karlstom, K., and Timmons, J.M., 2000, Inversion of Proterozoic extensional faults: An explanation for the pattern of Laramide and Ancestral rockies intracratonic deformation, United States: Geology, v. 28, no. 8, p. 735–738, doi: 10.1130/0091-7613(2000)28<735:IOPEFA>2.0.CO;2.

Matenaar, I.F., 2002, Compaction and microfabric rearrangement of fine-grained siliciclastic sediments: PhD Thesis, University of Newcastle-Upon-Tyne, UK, p. 253 pp.

Mathews, W.H., 1975, Cenozoic erosion and erosion surfaces of eastern North America: American Journal of Science, v. 275, p. 818–824, doi: 10.2475/ajs.275.7.818.

McCabe, C., Jackson, M., and Saffer, B., 1989, Regional Patterns of Magnetite Authigenesis in the Appalachian Basin: Implications for the Mechanism of Late Paleozoic Remagnetization: Journal of Geophysical Research, v. 94, no. B8, p. 429–443.

Middleton, G. V., 1973, Johannes Walther's Law of the Correlation of Facies: Bulletin of the Geological Society of America, v. 84, no. 3, p. 979–988, doi: 10.1130/0016-7606(1973)84<979:JWLOTC>2.0.CO;2.

Miller, J.D., and Kent, D. V, 1988, Regional trends in the timing of Alleghenian remagnetization in the Appalachians: Geology, v. 16, p. 588–591.

Mitra, S., 1987, Regional variations in deformation mechanisms and structural styles in the central Appalachian orogenic belt: Geological Society of America Bulletin, v. 98, no. 5, p. 569–590, doi: 10.1130/0016-7606(1987)98<569:rvidma>2.0.co;2.

This article is protected by copyright. All rights reserved.

Author Manuscript

Molnar, P., 1988, Continental tectonics in the aftermath of plate tectonics: Nature, v. 335, no. 6186, p. 131–137, doi: 10.1038/335131a0.

Momper, J.A., 1978, Oil Migration Limitations Suggested by Geological and Geochemical Considerations: v. 34, p. T.1-60.

Moore, D.M., and Reynolds, R.C.J., 1997, X-ray Diffraction and the Identification and Analysis of Clay Minerals: Oxford University Press, New York.

Morgan, W.J., 1968, Rises, Trenches, Great Faults and Crustal Blocks: Tectonophysics, v. 73, no. 6, p. 1959–1982, doi: 10.1016/0040-1951(91)90408-K.

Mulch, a., and Chamberlain, C.P., 2007, Stable Isotope Paleoaltimetry in Orogenic Belts The Silicate Record in Surface and Crustal Geological Archives: Reviews in Mineralogy and Geochemistry, v. 66, no. 1, p. 89–118, doi: 10.2138/rmg.2007.66.4.

Neprochnov, Y.P., Levchenko, O. V., Merklin, L.R., and Sedov, V. V., 1988, The structure and tectonics of the intraplate deformation area in the Indian Ocean: Tectonophysics, v. 156, no. 1–2, doi: 10.1016/0040-1951(88)90285-5.

Nickelsen, R.P., and Hough, V.N.., 1967, Jointing in the Appalachian Plateau of Pennsylvania: Geological Society of America Bulletin, v. 78, p. 609–630.

Nunn, A., and Deming, D., 1991, Thermal constraints on basin-scale flow systems: Geophysical Research Letters, v. 18, no. 5, p. 967–970.

Oliver, J., 1986, Fluids expelled tectonically from orogenic belts: Their role in hydrocarbon migration and other geologic phenomena: Geology, v. 14, no. 2, p. 99–102.

Olsen, P.E., 1997, Stratigraphic Record of the Early Mesozoic Breakup of Pangea in the Laurasia-Gondwana Rift System: Annual Review of Earth and Planetary Sciences, v. 25, no. 1, p. 337–401, doi: 10.1146/annurev.earth.25.1.337.

Person, M., and Baumgartner, L., 1995, New evidence for long-distance fluid migration within the Earth's crust: Reviews of Geophysics, v. 33, no. 2 S, p. 1083–1091, doi: 10.1029/95RG00254.

This article is protected by copyright. All rights reserved.

Author Manuscript

Peyser, C.E., and Poulsen, C.J., 2008, Controls on Permo-Carboniferous precipitation over tropical Pangaea: A GCM sensitivity study: Palaeogeography, Palaeoclimatology, Palaeoecology, v. 268, no. 3–4, p. 181–192, doi: 10.1016/j.palaeo.2008.03.048.

Poulsen, C.J., Pollard, D., Montañez, I.P., and Rowley, D., 2007, Late Paleozoic tropical climate response to Gondwanan deglaciation: Geology, v. 35, no. 9, p. 771–774, doi: 10.1130/G23841A.1.

Quinlan, G.M., and Beaumont, C., 1984, Appalachian thrusting, lithospheric flexure, and the Paleozoic stratigraphy of the Eastern Interior of North America: Canadian Journal of Earth Sciences, v. 21, no. 9, p. 973–996, doi: 10.1139/e84-103.

Reed, J.S., Spotila, J.A., Eriksson, K.A., and Bodnar, R.J., 2005, Burial and exhumation history of Pennsylvanian strata, central Appalachian basin: An integrated study: Basin Research, v. 17, no. 2, p. 259–268, doi: 10.1111/j.1365-2117.2005.00265.x.

Ryder, R.T., Crangle, R.D., J., Trippi, M.H., Swezey, C.S., Lentz, E.E., Rowan, E.L., and Hope, R.S., 2009, Geologic cross section D–D' through the Appalachian basin from the Findlay arch, Sandusky County, Ohio, to the Valley and Ridge province, Hardy County, West Virginia: U.S. Geological Survey Scientific Investigations Map 3067, v. 2 sheets, no. 52–pamphlet.

Samson, S.D., and Alexander, E.C., 1987, Calibration of the interlaboratory 40Ar39Ar dating standard, MMhb-1: Chemical Geology: Isotope Geoscience Section, v. 66, no. 1–2, p. 27–34, doi: 10.1016/0168-9622(87)90025-X.

Schedl, A., 1992, Non-Darcian fluid flow during the Alleghenian Orogeny: Earth and Planetary Science Letters, v. 113, p. 511–519.

Schedl, A., McCabe, C., Montanez, I., Fullagar, P.D., and Valley, J.W., 1993, Alleghenian regional diagenesis: A response to the migration of modified metamorphic fluids derived from beneath the Blue Ridge-Piedmont thrust sheet: The Journal of Geology, v. 100, no. 3, p. 339–352.

Schemmel, F., Mikes, T., Rojay, B., and Mulch, A., 2013, The impact of topography on isotopes in precipitation across the Central Anatolian Plateau (Turkey): American Journal of Science, v. 313, no. 2, p. 61–80, doi: 10.2475/02.2013.01.

This article is protected by copyright. All rights reserved.

Author Manuscript

Sheppard, S.M.F., 1986, Characterization and isotopic variations in natural waters: Reviews in Mineralogy, v. 16, p. 165–184.

Sibson, R.H., 2005, Hinge-parallel fluid flow in fold-thrust belts: how widespread? Proceedings of the Geologists' Association, v. 116, no. 3–4, p. 301–309, doi: 10.1016/S0016-7878(05)80048-3.

Singh, S.C., Hananto, N., Qin, Y., Leclerc, F., Avianto, P., Tapponnier, P.E., Carton, H., Wei, S., Nugroho, A.B., Gemilang, W.A., Sieh, K., and Barbot, S., 2017, The discovery of a conjugate system of faults in the Wharton Basin intraplate deformation zone: Science Advances, v. 3, no. 1, p. e1601689, doi: 10.1126/sciadv.1601689.

Slingerland, R., and Furlong, K.P., 1989, Geodynamic and Geomorphic Evolution of the Permo-Triassic Appalachian Mountains: Geomorphology, v. 2, p. 23–37.

Stamatakos, J., Hirt, A.M., and Lowrie, W., 1996, The age and timing of folding in the central Appalachians from paleomagnetic results: Geological Society of America Bulletin, v. 108, no. 7, p. 815–829, doi: 10.1130/0016-7606(1996)108<0815:TAATOF>2.3.CO;2.

Sverjensky, D.A., 1986, Genesis of Mississippi Valley-Type Lead-Zinc: Ann. Rev. Earth Planet. Sci, v. 147, no. 1, p. 7–99, doi: 10.1146/annurev.earth.14.1.177.

Torsvik, T.H., Carlos, D., Mosar, J., Cocks, L.R.M., and Malme, T.N., 2002, Global reconstructions and North Atlantic paleogeography 440 Ma to recent: BATLAS—Mid-Norway plate reconstruction atlas with global and Atlantic perspectives, p. 18–39.

Townend, J., and Zoback, M., 2000, How faulting keeps the crust strong: Geology, v. 28, no. 5, p. 399-402, doi: 10.1130/0091-7613(2000)28<399.

van der Pluijm, B., Craddock, J., Graham, B., and Harris, J., 1997, Paleostress in cratonic North America: Implications for deformation of continental interiors: Science, v. 277, no. August, p. 794–796.

van der Pluijm, B.A., and Hall, C., 2015, Brittle Fault Dating, in Encyclopedia of Scientific Dating Methods, Springer, New York.

This article is protected by copyright. All rights reserved.

Author Manuscript

van der Pluijm, B.A., Hall, C.M., Vrolijk, P.J., Pevear, D.R., and Covey, M.C., 2001, The dating of shallow faults in the Earth's crust.: Nature, v. 412, no. 6843, p. 172–5, doi: 10.1038/35084053.

van der Pluijm, B.A., Ho, N., and Peacor, D., 1994, High-resolution X-ray texture goniometry: Journal of Structural Geology, v. 16, no. 7, p. 1029–1032.

Vander Voo, R., 1988, Paleozoic paleogeography of North America, Gondwana, and intervening displaced terranes: Comparisons of paleomagnetism with paleoclimatology and biogeographical patterns: Bulletin of the Geological Society of America, v. 100, no. 3, p. 311–324, doi: 10.1130/0016-7606(1988)100<0311:PPONAG>2.3.CO;2.

Vander Voo, R., and Torsvik, T.H., 2012, The history of remagnetization of sedimentary rocks: deceptions, developments and discoveries: Geological Society, London, Special Publications, v. 371, no. 1, p. 23–53, doi: 10.1144/SP371.2.

Zoback, M.D., and Townend, J., 2001, Implications of hydrostatic pore pressures and high crustal strength for the deformation of intraplate lithosphere: Tectonophysics, v. 336, no. 1–4, p. 19–30, doi: 10.1016/S0040-1951(01)00091-9.

This article is protected by copyright. All rights reserved.

Author Manuscript

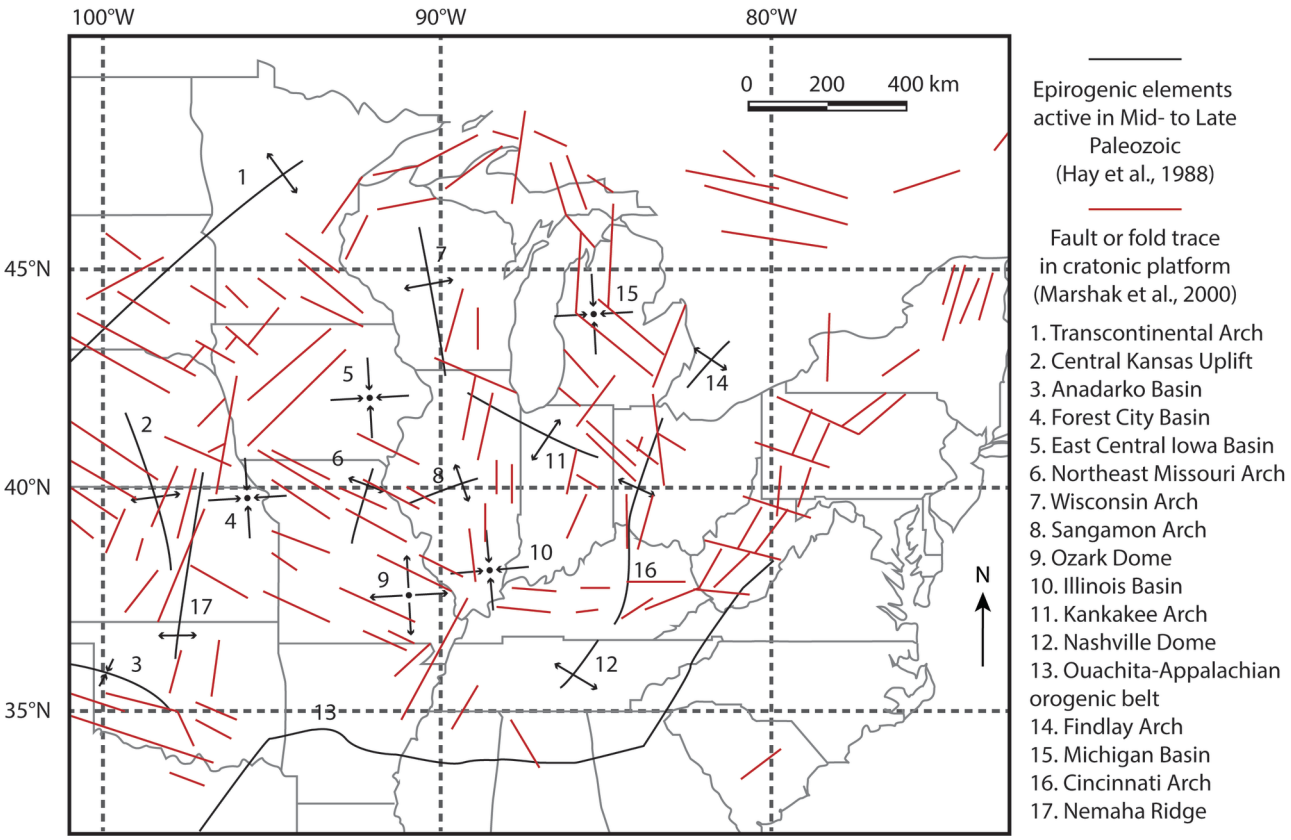

2020TC006137-f01-z-.tif

This article is protected by copyright. All rights reserved.

Author Manuscript

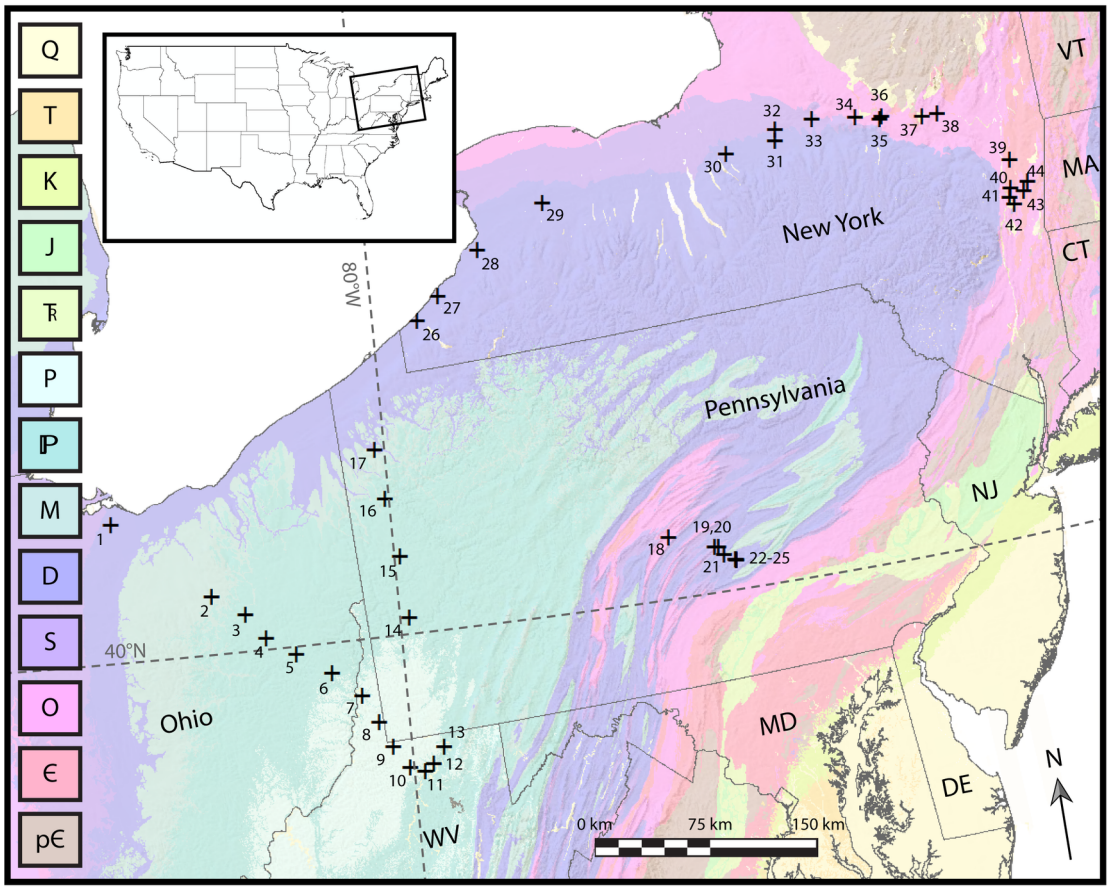

1. OH06 (IECLA0010)
2. OH05* (IECLA000Z)
3. OH04* (IECLA000Y)
4. OH03 (IECLA000X)
5. OH02* (IECLA000W)
6. OH01 (IECLA000V)
7. WV07* (IECLA000U)
8. WV06 (IECLA000T)
9. WV05* (IECLA000S)
10. WV04 (IECLA000R)
11. WV03 (IECLA000Q)
12. WV02 (IECLA000P)
13. WV01* (IECLA000O)
14. PA04* (IECLA000N)
15. PA03 (IECLA000M)
16. PA02 (IECLA000L)
17. PA01* (IECLA000K)
18. SNPA8* (IECLA0018)
19. SNPA7* (IECLA0017)
20. SNPA6 (IECLA0016)
21. SNPA5 (IECLA0015)
22. SNPA4 (IECLA0014)
23. SNPA3* (IECLA0013)
24. SNPA2 (IECLA0012)
25. SNPA1 (IECLA0011)
26. NY01 (IECLA0001)
27. NY02* (IECLA0002)
28. NY03 (IECLA0003)
29. NY04* (IECLA0004)
30. NY05 (IECLA0005)
31. NY06 (IECLA0006)
32. NY07* (IECLA0007)
33. NY08 (IECLA0008)
34. NY19* (IECLA000J)
35. NY09 (IECLA0009)
36. NY10 (IECLA000A)
37. NY11 (IECLA000B)
38. NY12 (IECLA000C)
39. NY13 (IECLA000D)
40. NY14 (IECLA000E)
41. NY15* (IECLA000F)
42. NY16 (IECLA000G)
43. NY17 (IECLA000H)
44. NY18 (IECLA000I)

2020TC006137-f02-z-.tif

This article is protected by copyright. All rights reserved.

Author Manuscript

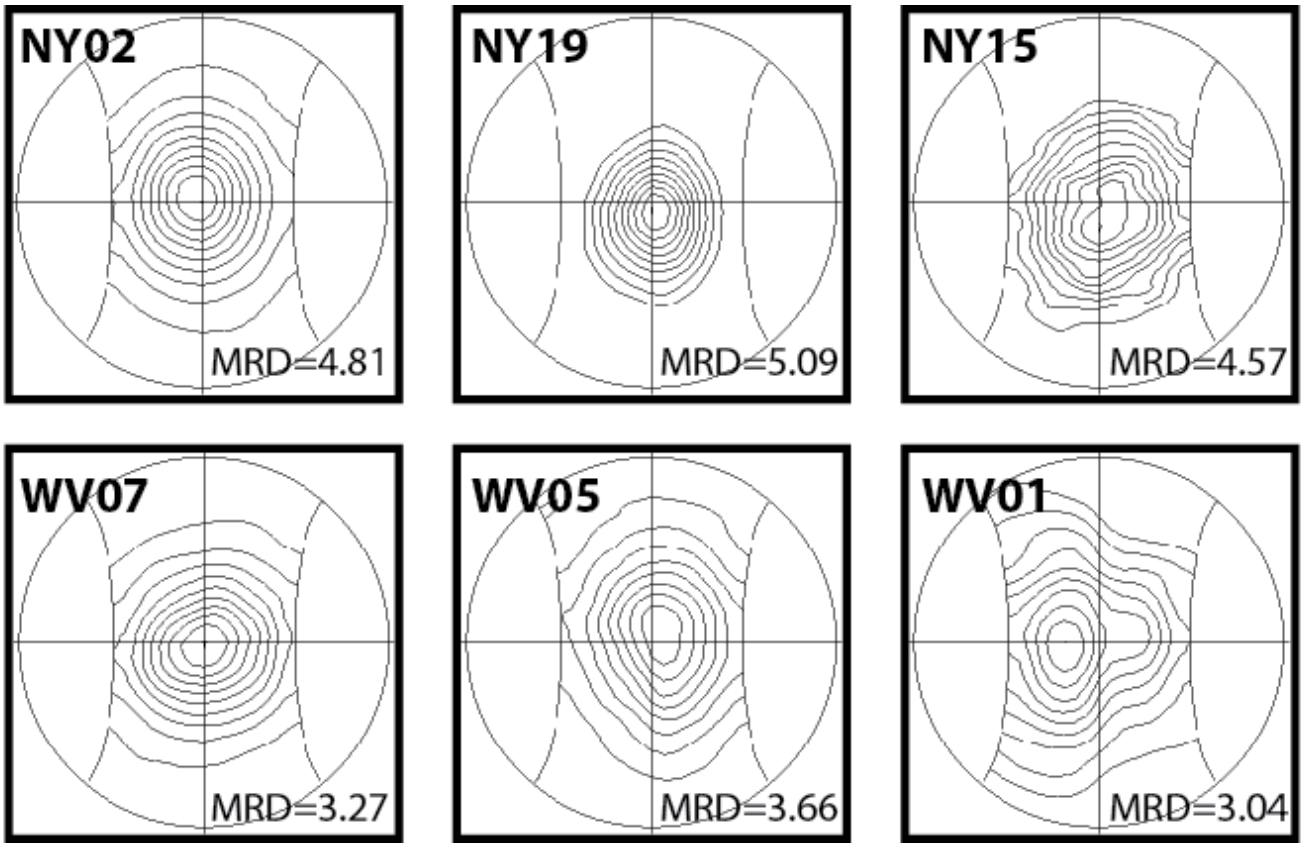

2020TC006137-f03-z-.png

This article is protected by copyright. All rights reserved.

Author Manuscript

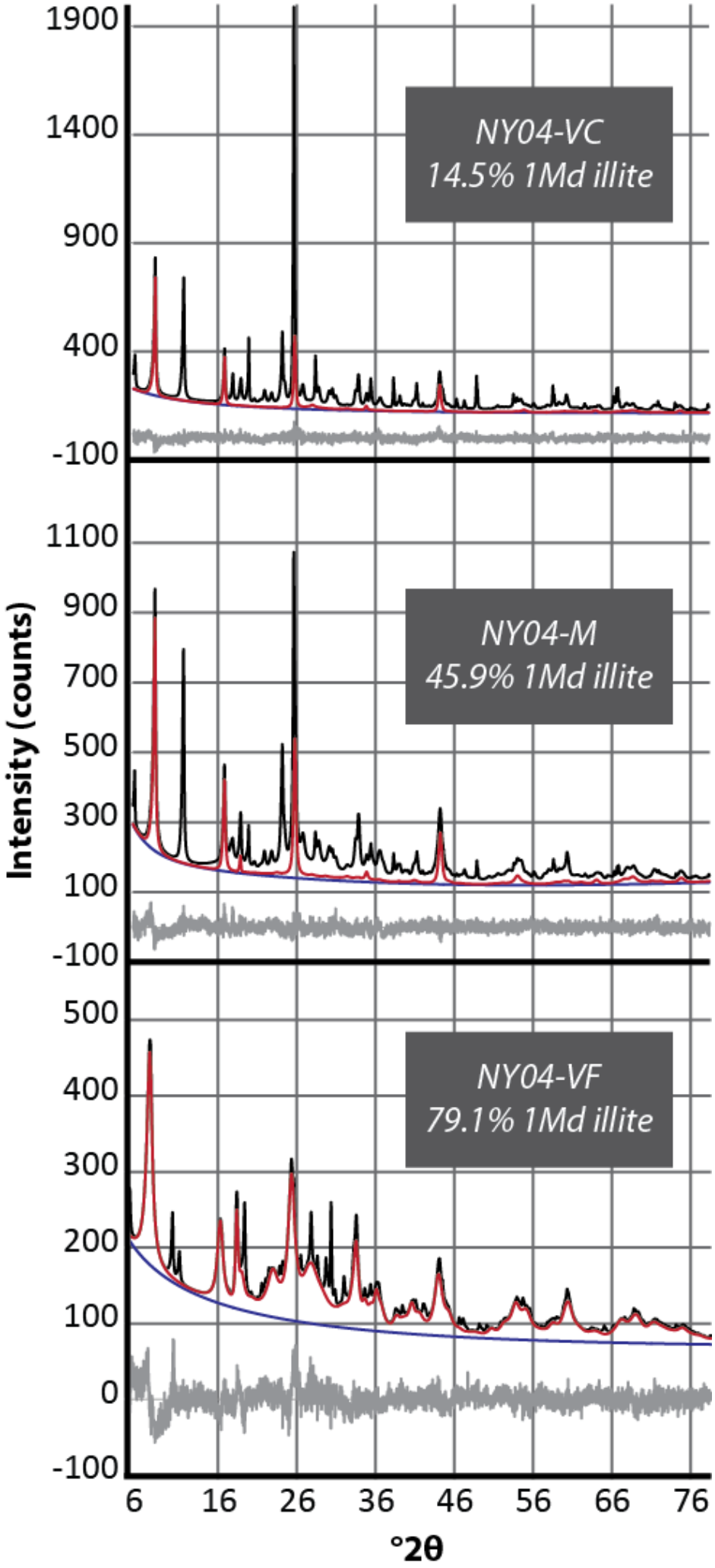

2020TC006137-f04-z-.png

This article is protected by copyright. All rights reserved.

Author Manuscript

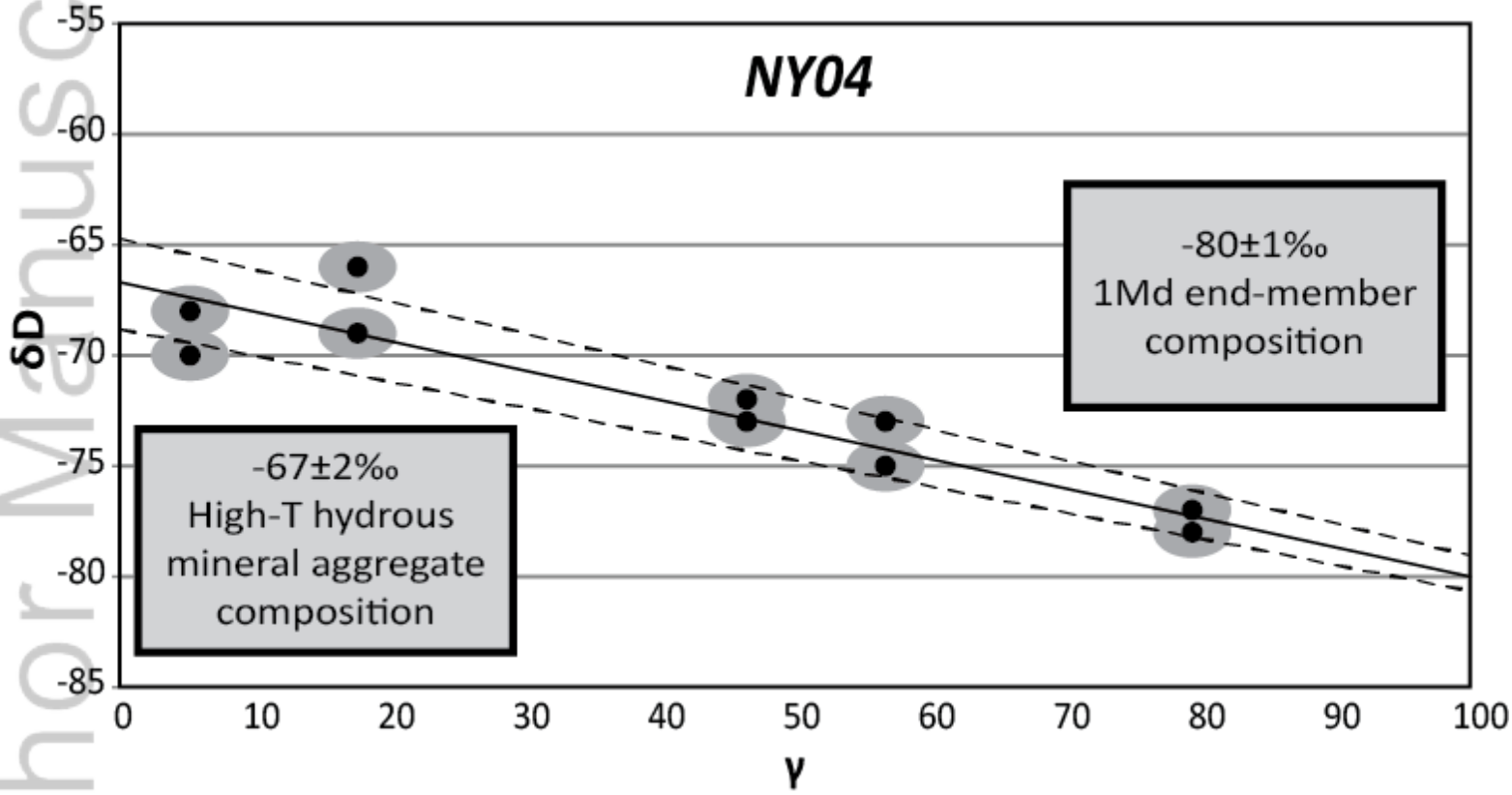

2020TC006137-f05-z-.png

This article is protected by copyright. All rights reserved.

Author Manuscript

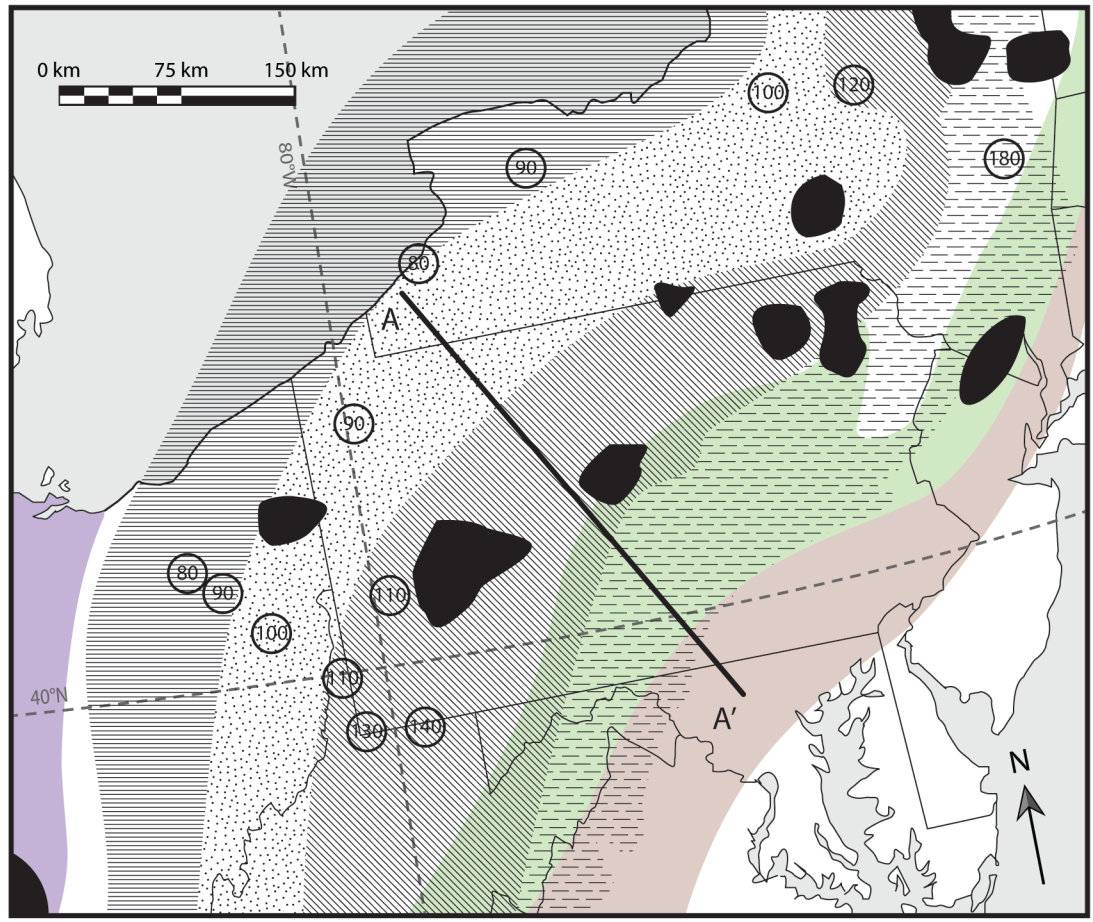

2020TC006137-f06-z-.tif

This article is protected by copyright. All rights reserved.

Author Manuscript

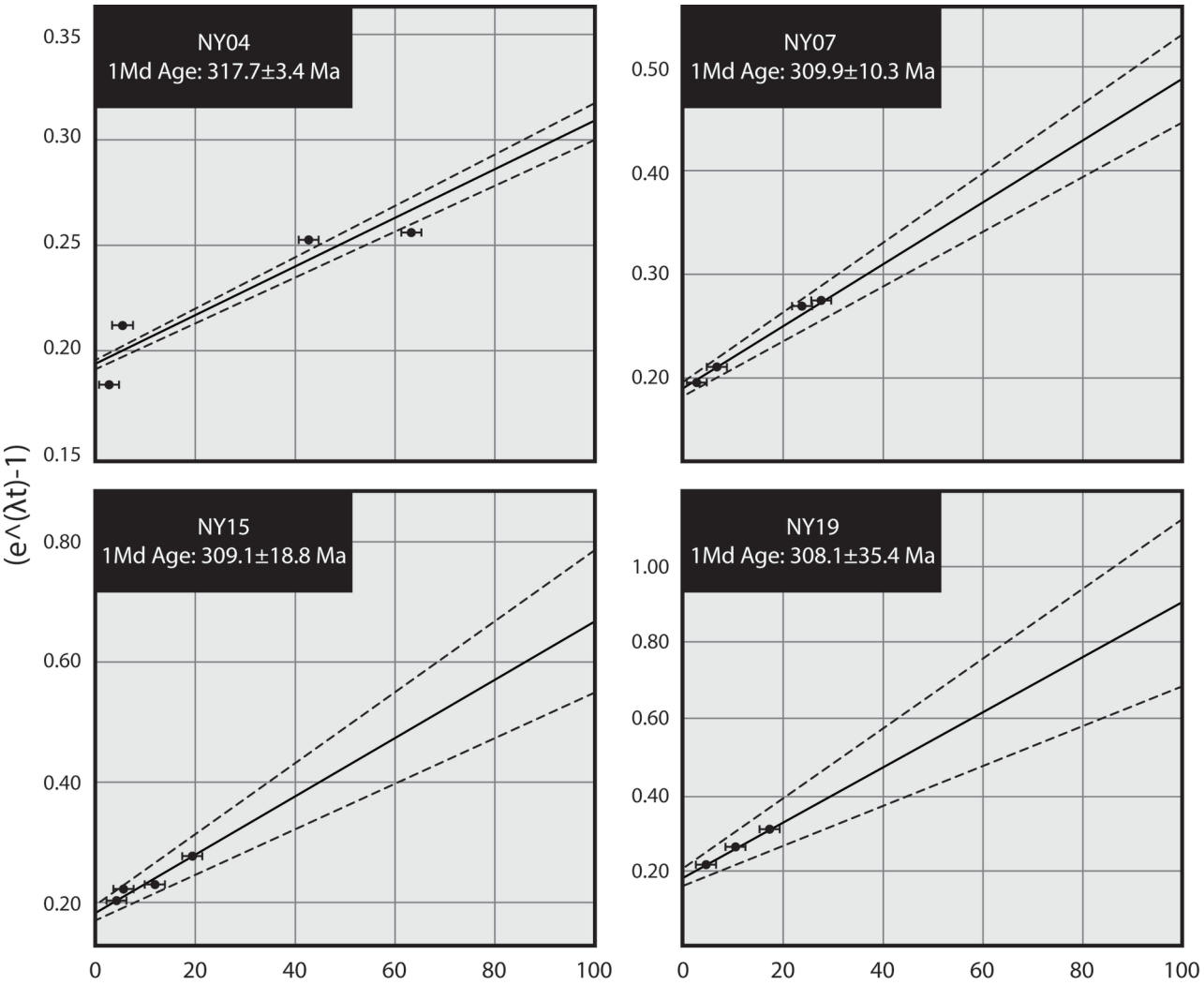

2020TC006137-f07-z-.tif

This article is protected by copyright. All rights reserved.

Author Manuscript

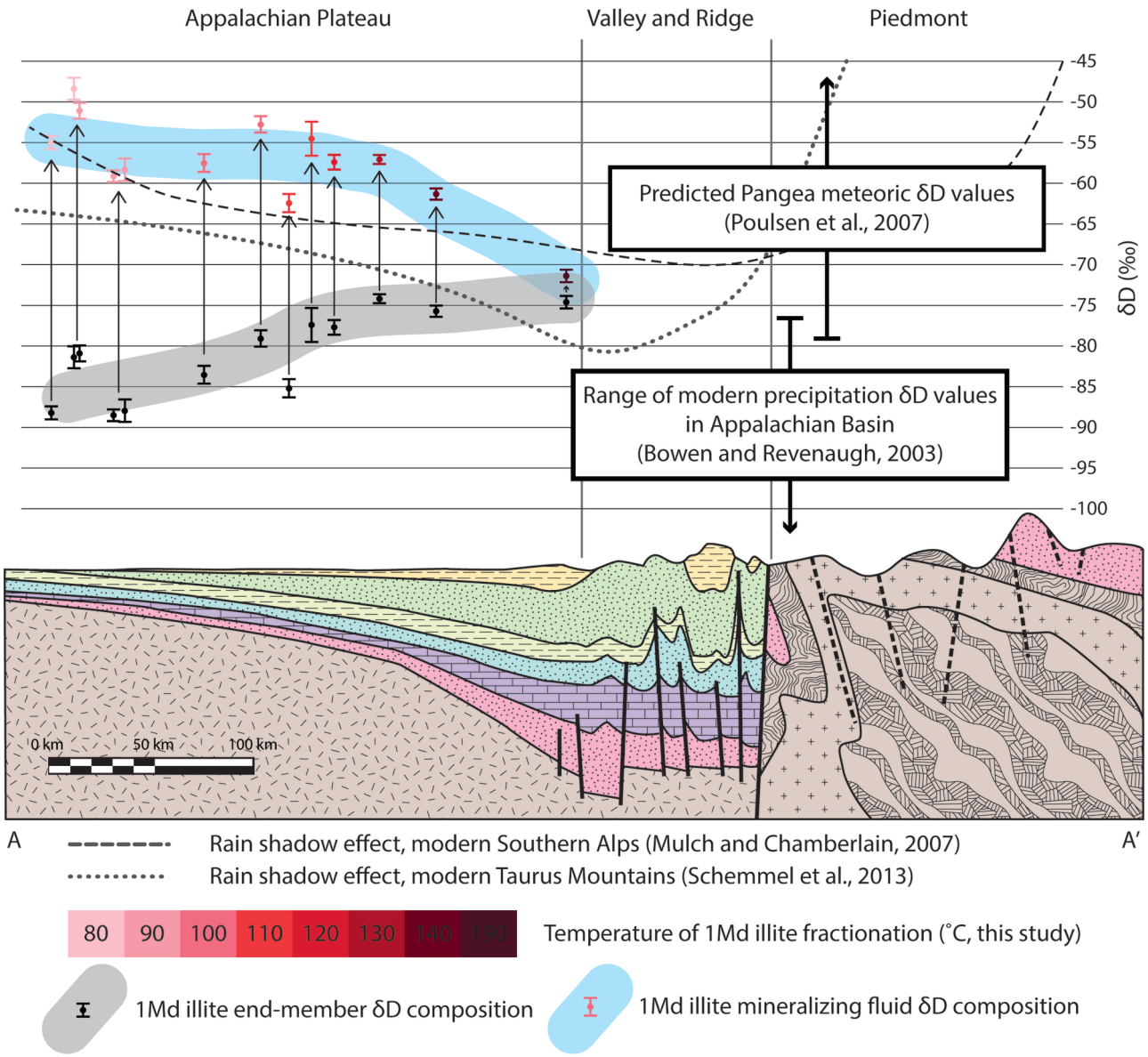

2020TC006137-f08-z-.tif

This article is protected by copyright. All rights reserved.

Author Manuscript

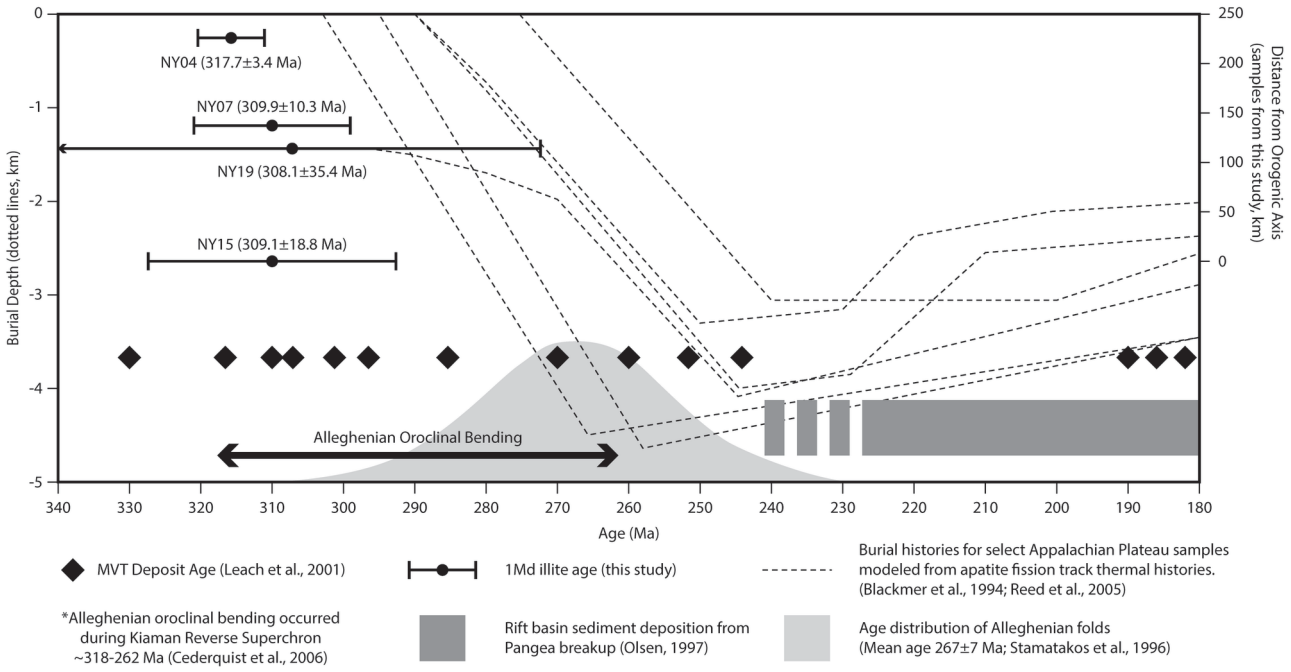

2020TC006137-f09-z-.tif

This article is protected by copyright. All rights reserved.